Stony Brook University

OFFICIAL COPY

The official electronic file of this thesis or dissertation is maintained by the University Libraries on behalf of The Graduate School at Stony Brook University.

© All Rights Reserved by Author.

On the Fracture Toughness and Crack Growth Resistance of Bio-Inspired Thermal Spray Hybrid Composites

A Thesis Presented

by

Michael Murray Resnick

to

The Graduate School

in Partial Fulfillment of the

Requirements

for the Degree of

Master of Science

In

Materials Science and Engineering

Stony Brook University

May 2016

Stony Brook University

The Graduate School

Michael Murray Resnick

We, the thesis committee for the above candidate for the

Master of Science degree, hereby recommend

acceptance of this thesis.

Dr. Sanjay Sampath – Thesis Advisor
Professor, Materials Science and Engineering

Dr. Gopal Dwivedi – Second Reader
Research Scientist, Materials Science and Engineering

This thesis is accepted by the Graduate School

Charles Taber
Dean of the Graduate School

Abstract of the Thesis

On the Fracture Toughness and Crack Growth Resistance of Bio-Inspired Thermal Spray Hybrid Composites

by

Michael Murray Resnick

Master of Science

in

Materials Science and Engineering

Stony Brook University

2016

Nature has presented a remarkable bill of materials which show excellent mechanical properties. Among those which have been extensively studied are wood, bone, rocks, spider silk, nacre etc. Interestingly all of these materials are primarily known to have great fracture resistance and present excellent example of natural and layer-by-layer evolution of materials. These materials have inspired the current research society to synthesize new generation materials with mechanical properties beyond the conventional materials such as metal, ceramic and polymers. Nacre, one of the most researched natural materials, is present in particular sea-shells and shows a layered brick-and-mortar structure. Designing nacre-like structures has been a goal of many researchers due to the combination of its high strength and toughness.

Thermal spray, a melt deposition process, has the ability to produce similar structures which can exhibit mechanical behavior similar to nacre. With an appropriate selection of process conditions, a nacreous brick-&-mortar structure can be synthesized. The structure is consisting of 95 vol% of $CaCO_3$ tablets with a brick wall arrangement with 5vol% of bio-polymer serving as a mortar between tables. Although, there have been several attempts by other researchers in the past, many other attempts have been made to synthesize such a material, they remain limited to a laboratory scale dimensions and are challenging to be scalable. While thermal spray, a readily scalable and industrially adapted process, shows no limitations with the development of nacre-like structures over a large surface area.

Previous work down by the group has produced such a nacre-like structure using a flame spray process, one of the variant of thermal spray which uses rod as a feed, resulted in similar mechanical behavior to that of nacre. The work demonstrated that these templates along with the introduction of a polymeric epoxy, the fracture toughness and strength can be raised up to the values of a real nacre. Although, the fracture toughness was primary property of this study and the values were well matched, the fracture behavior found to be somewhat different between the hybrid composite and nacre. In particular, the hybrid composite was unable to exhibit any

significant toughness under slow crack growth conditions, which is the most attractive feature of nacre.

This thesis focuses on first investigating the toughness in the sprayed hybrid composites by using standard resistance curve (R-curve) measurements. The study then focused on developing thermal spray modified hybrid composites with improved toughness, as well as with higher application temperatures, beyond the limitation of epoxy.

This thesis is dedicated to my parents.

For all their love, support, and sacrifice over the years. All my accomplishments are because of everything you have done for me. I love you both very much.

Table of Contents

List of Figures

Acknowledgments

I would first like to acknowledge both Professor Sanjay Sampath and Dr. Gopal Dwivedi for giving me the opportunity to join the Center for Thermal Spray Research and help discover my passion for both thermal spray and materials science and engineering. Over the years at being at CTSR, they have taught me so much, but most importantly, saw potential in me that I did not think I even had. Thanks to my mentors, I took the opportunity to pursue my Master's Thesis and gained further knowledge, experience, and confidence in my abilities.

I would also like to acknowledge all the other wonderful people at CTSR, who I can happily say, are all my friends. Thank you all for the support, help, and wisdom you have given me at my time here.

1. Introduction

From a materials point of view, there has always been a competition between fracture toughness and fracture strength. In general, high fracture toughness is typically desired over that of high strength, if the material is considered for structural applications which involves mechanical loadings. Materials that have only high strength, and hence low fracture toughness will experience catastrophic failure, while materials with a high toughness will have a strong resistance against failure in the presence of a crack. A desired structural material is required to have intrinsic toughness so if during service any crack propagation is not sudden and is rather slow (stable) to avoid catastrophic failure. Several research studies have been dedicated to understand the fracture mechanisms of various materials which has led to identify the class of materials most suitable for any structural applications. The following sections of this chapter has been designed to address the understanding, mechanisms and associated various measurement techniques to address fracture in a material.

1.1. Fracture toughness and crack growth resistance

Fracture toughness is a material's ability to resist fracture once a crack is present [1]. Fracture toughness can be determined by using the stress intensity factor (K) at the crack tip. A fracture in a material occurs when this stress intensity factor approaches its critical value, which is referred to as the critical stress intensity factor (K_c), or the fracture toughness.

$$Kc = \sigma_c\sqrt{\pi a}\ (1.1)\ [1]$$

Equation 1.1 above, shows the general equation for calculating fracture toughness with K where σ_c is the critical stress, **π** is the value for pi and a is the length of the crack. In some cases, a dimensionless parameter (Y) is used that varies based on the size, geometries, application of load of specimen [2]. This equation is derived from the stress fields at the crack tip and the assumption that there is a through-thickness crack in an infinite plate being loaded in biaxial tension. K additionally, is notated with either I, II, or III subscript depending on the mode of fracture as shown in Figure 1.1. Mode I is opening (tensile stress normal to plane of crack), mode II is in-plane shear (parallel to plane of crack and perpendicular to crack front), and mode III is out-of-plane shear (parallel to plane of crack and crack front)[2].

Typically, there is a correlation between fracture toughness and fracture behavior, as shown in Figure 1.2 [1]. Materials with low fracture toughness exhibit only a linear-elastic fracture mechanics meaning that upon loading/unloading, no change in the slope will occur. Additionally, this signifies that upon failure no plastic deformation occurs and no resistance will initiate upon crack growth. Once the fracture toughness of materials goes beyond this point, linear-elastic fracture mechanics is not effective since a material now undergoes plastic deformation. This is demonstrated when a change in the slope occurs since the plastic deformation allows energy to be released or consumed by several contributing factors, causing resistance upon crack initiation. In some cases, materials with extraordinary high fracture toughness cannot be determined with

fracture toughness and only limit-load analysis can be completed. Materials such as ceramics and high strength metals will not experience plastic deformation due to the high stiffness present. Other class of materials experience non-linear behavior or elastic plastic behavior that has higher fracture toughness values. This includes low and medium strength metals since plastic deformation does occur with these materials. Further, polymeric materials exhibit plastic deformation which can have high toughness but not to the extent of metals.

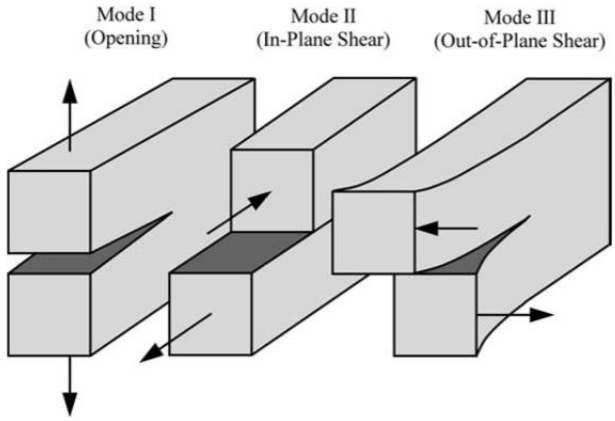

Figure 1.1: Diagrams for each mode of fracture [1].

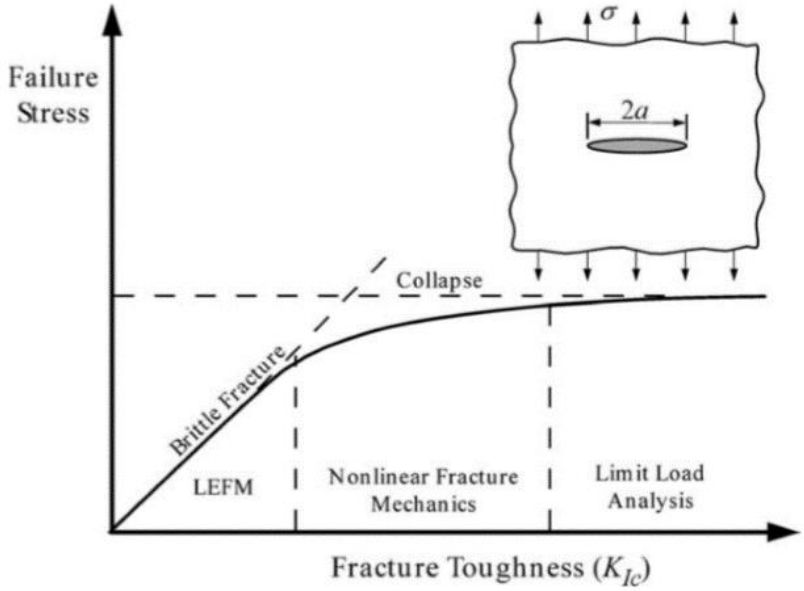

Figure 1.2 Diagram showing the various types of fracture behavior based on fracture toughness with a diagram of fracture stress for a penny shaped flaw in a material. [1]

While fracture toughness (K_c) is useful and gives some information about fracture behavior of materials, it does not give the full picture [1]. More detailed information about the fracture behavior comes in the form of the crack growth resistance curves (R-Curve) which is generally represented as the energy release rate (G) of a material with respect to associated extension of the crack (J-R Plot)[3]. A material exhibiting a stable and slower crack growth is considered to

possess higher toughness. The J-R plot essentially tells us the work required for a crack to propagate at successive notch extensions and the shape of this curve determines the toughness of the material.

Materials either experience a flat or rising R-curve as shown in Figure 1.3[1]. A flat R-curve (left image) occurs when no additional energy (constant) or work is required as the crack propagates. At the initial stress ($\boldsymbol{\sigma}_1$) there is crack stability but once $\boldsymbol{\sigma}_2$ is reached, fracture initiates, becoming unstable since the driving force is increasing as the crack extends at constant resistance. Rising R-curve (right image) is when there is a change in resistance as the crack propagates. At $\boldsymbol{\sigma}_2$, the stress becomes fixed at a slower rate than that of the resistance. Stable crack growth continues to stay constant up to $\boldsymbol{\sigma}_3$ and once it reaches $\boldsymbol{\sigma}_4$, the driving forces becomes tangential to the curve. This signifies that the material becomes unstable with any crack growth at this point when change in driving forces overcomes the slope of the curve.

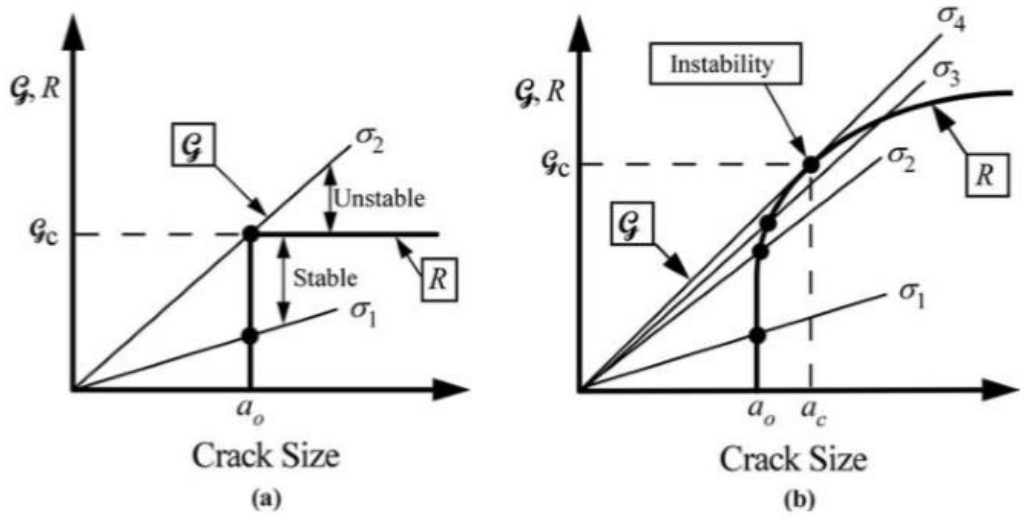

Figure 1.3 Diagram showing (a) a material with no crack growth resistance and (b) a material that does exhibit crack growth resistance. [1]

The type of R-curve behavior that occurs is dependent on the intrinsic or extrinsic toughening mechanisms.[4]. Intrinsic toughening is correlated with enhancement of toughness with the increase in the overall fracture resistance from the microstructure. This is accomplished through changing the nature, distribution, and/or interface properties of second-phase particles. This results in the suppression of damage ahead of the crack top from microcracking or microvoid formation. Such microstructural developments are commonly seen in ductile materials such as metallics, in which their toughness is stemmed from.

Ceramics, on the other hand, do not have this intrinsic toughening and therefore, rely on extrinsic toughening mechanisms. These mechanisms do not influence the crack initiation of the material, rather act behind the crack tip to reduce the crack-driving force that is experienced at the crack tip. [4]. This is also called crack-tip shielding which occurs from mechanisms such as crack bridging and in situ phase transformations. Figure 1.4 illustrates the various mechanisms associated with the intrinsic and extrinsic toughening. In the case of R-curve, a flat behavior is experienced when a material only has intrinsic toughening, while a rising behavior occurs when extrinsic toughening is occurring. The rising R-curve indicates that the crack experiences increasing resistance with propagation, which is a) a results of extrinsic toughening

(behind/wake of the crack), b) dependent on the flaw size which is why it is plotted as notch extension and not notch size [4]. Figure 1.5 demonstrates the various extrinsic toughening mechanisms that occur in the material with rising R-curve. It is also important to understand that this behavior is not crack resistance. Crack resistance is property of the material that comes from intrinsic toughening (front of the crack) and is independent of flaw size. In general crack resistance is closely related to the fracture toughness of the material.

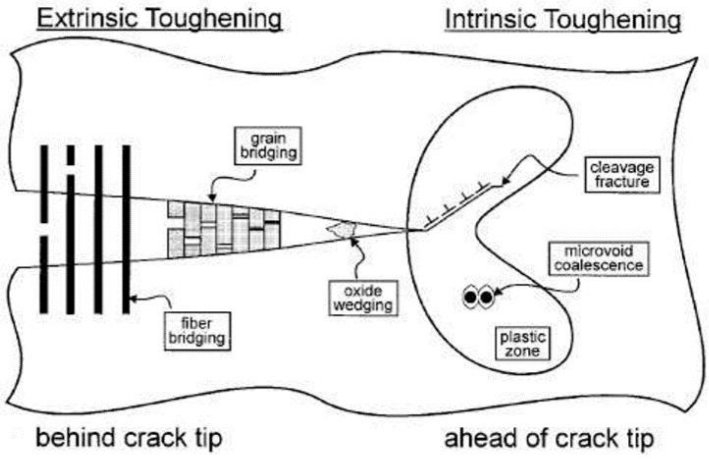

Figure 1.4: Diagram showing extrinsic and intrinsic toughening with examples of different mechanisms involved with each.[4]

1.2.Methods to test for fracture toughness

There are several standards which have been developed in the past to measure the fracture toughness and resistance of materials under different fracture modes. However, the majority of those are to perform the measurements in Mode-I. As per ASTM (E399) there are five common specimen dimensions for mode-I fracture toughness measurement methods as shown in Figure 1.6 [1, 5]. They are single edge notch bend, compact specimen, arc shaped specimen, disk specimen, and middle tension. Each test has their own specimen dimension and notching requirements. For the single edge notch bend, a 3-point bend configuration is used which lays a flat specimen positioned on two rollers while the third roller applies a downward force on the center opposite of were the notch is located. Compact, disk shaped, and arc-shaped specimen use an apparatus that uses pins to hold the sample and applies a load on the center opposite of were the notch is located. Middle tension involves a notch positioned in the middle of the specimen where a tensile load is applied in opposite directions.

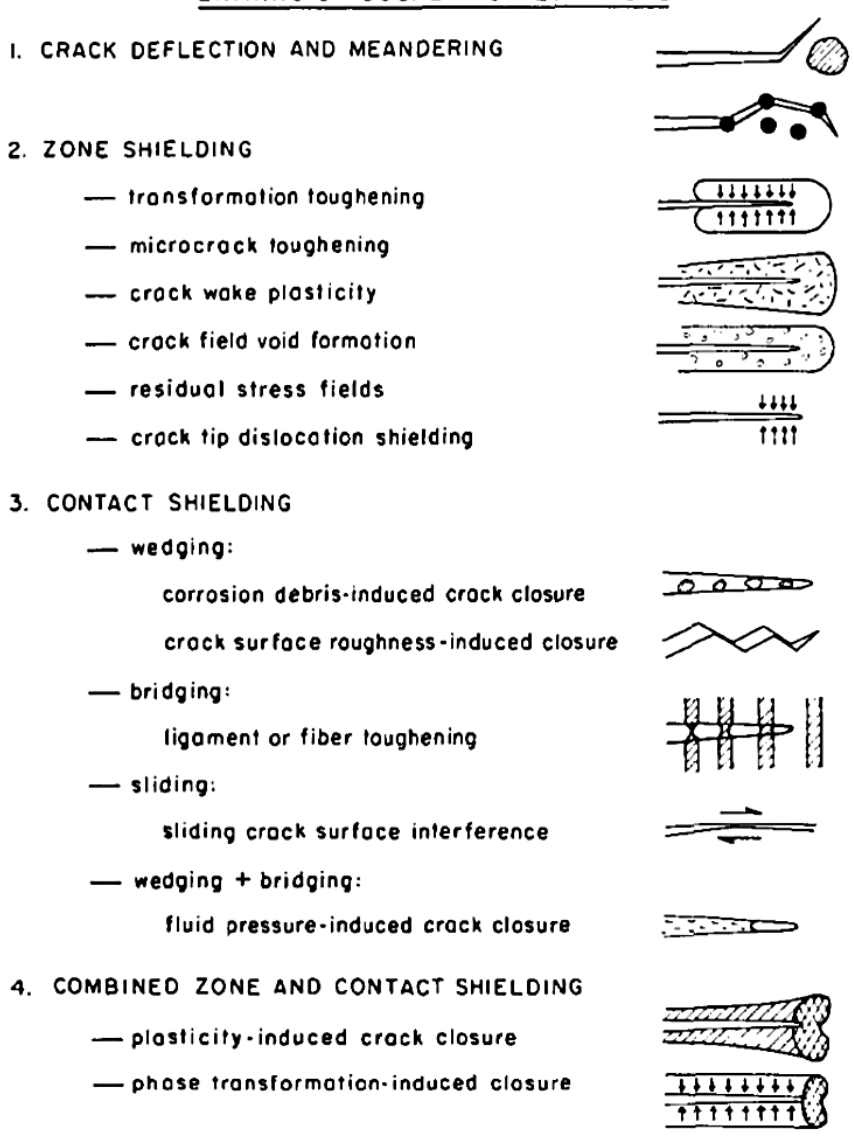

Figure 1.5: Diagram listing and demonstrating all the various extrinsic toughening mechanism. [6]

Compact specimen testing is advantageous since it uses less material but since the holes are needed for the pins, the material has to have a significant width to compensate for it [1]. In addition, due to requirements of holes, ceramics are difficult to be considered for such a test. In fact, the same restrictions are present for other fracture toughness testing, except for middle tension and single edge notch bend (SENB) testing, but SENB is more common for ceramic fracture testing. This method also is more advantageous since the specimen size has more flexibility and allows a few alterations in the test methods, such as change is load span without any additional specimen preparation requirement.

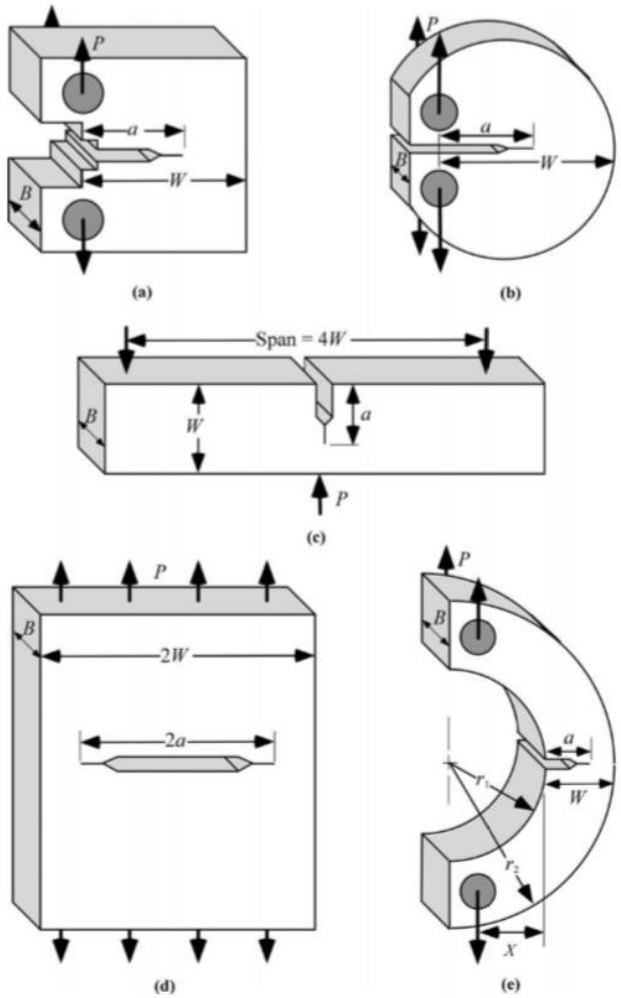

Figure 1.6:Schematic for (a) compact specimen, (b) disk shaped compact specimen, (c) single edge notch bend specimen, (d) middle tension specimen, and (e) arc shaped specimen.[1]

While testing for fracture toughness, it is assumed that there is an infinitely sharp notch with a radius of the scale of lattice dimensions, which realistically is not feasible [1]. Therefore, a notch radius of few microns is acceptable which, for metals, is produced through fatigue sequence. However, for ceramics, since fatigue is not possible, sharpening of notch using some sharp-edge device, such as a razor blade, is adopted.

1.3.Fracture behavior of metals, polymers, and ceramics & ceramic composites

Metals

Metals typically experience three types of fracture: ductile, cleavage, and intergranular fracture as demonstrated in Figure 1.7 [1]. During ductile fracture, three common stages occur.

1. Formation of a free surface at an inclusion or second-phase particle by either interface decohesion or particle cracking.

2. Growth of the void around the particle, by means of plastic strain and hydrostatic stress
3. Coalescence of the growing void with adjacent voids.

In order for voids to form in a pure metal there needs to be either a second-phase particle or inclusion with enough stress has to be applied to break bonds between the particle and matrix. Once the voids are present, they can continue to grow and coalesce. After the voids coalesce at the tip of the pre-crack and the cracked structure is loaded, local strains and stresses build up at the crack tip producing more voids. The voids continue to grow as the crack blunts and start to link with the main crack. This process continues as the crack grows. This crack growth is slow and making metals most reliable for structural application.

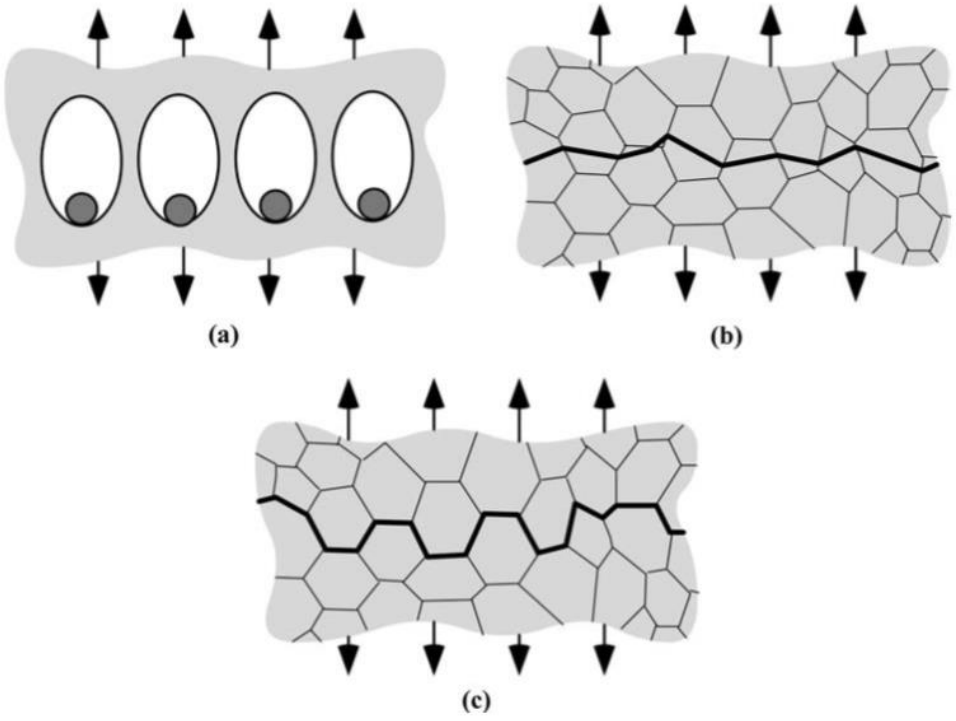

Figure 1.7: Schematics of (a) ductile fracture (b) cleavage, and (c) intergranular fracture[1]

Cleavage fracture in metals occurs with the rapid crack growth along a certain crystallographic plane [1]. This type of fracture is at first brittle, but can then be followed by large-scale plastic flow and ductile crack growth. This happens at planes where the packing density is the lowest, where there are less bonds to break and the spacing between the planes is greater. When the crack continues to propagate, it will choose the path with the least resistance. This happens by the crack switching direction as it approaches a different grain boundary.

More commonly, metals experience either one of the previous mentioned types of failure [1]. However intergranular fracture happens when a crack appears and grows along grain boundaries. This type of fracture happens in a variety of ways, which results in brittle failure.

1. Precipitation of a brittle phase on the grain boundary.
2. Environmental assisted cracking.
3. Intergranular corrosion.
4. Grain boundary cavitation and cracking at high temperatures.

Unlike other types of fracture that results from the material's structure, intergranular occurs due to extrinsic effects mentioned above. Brittle phases form from improper tempering. Environmental assisted cracking happens when at the crack tip, corrosion or hydrogen embrittlement occurs. Intergranular corrosion, unlike general corrosion stated previously, initiates only at grain boundaries.

Polymers

Polymers similar to that of metals, experience both ductile and brittle failure mechanisms [1]. However, the manner in which they occur are different. Polymers do not have crystallographic planes, dislocations, and/or grain boundaries and instead contain long repeating polymeric chains. Even with different ways of fracture, it still happens on the fundamental level of bonds breaking. The type of bonds that are with polymers are bonds with carbon atoms and van der Waal forces where the polymer will stretch but experiences more resistance due to the van der Waal forces attempting to keep the chains from moving. Strain rate, temperature, and molecular structure are the key factors that determine how tough and ductile the polymer will be. Brittle fracture can occur with high strain rates, low temperatures relative to glass transition temperature, and high amounts of cross-linking since these conditions will inhibit the polymers ability to deform by viscoelasticity.

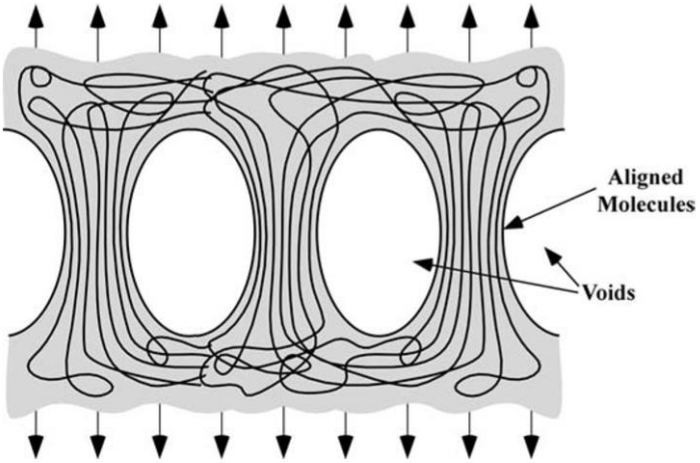

Figure 1.8: Schematic of crazing in polymers. [1]

Fracture in polymers can occur in a multitude of ways [1]. This includes chain scission, disentanglement, shear yielding, and crazing. Chain scission is fracture of the atomic level due to flaws occurring from the non-uniformity in the polymer's molecules when stress is applied. However, if the polymer is more crystalline than amorphous, the stress will be distributed more uniformly. Chain disentanglement, is when molecules separate while still remaining intact. The length and cross-linking of the polymer will determine how much this will occur.

Similarly to metals, polymers experience shearing except it does not occur in the same manner [1]. Shear yielding polymers have plastic flow like metals but does not occur on slip planes. Molecules slide with one another with polymers when the critical shear stress is reached. When it comes to glossy polymers, crazing can occur. Crazing is when voids form with high strain causing highly localized deformation as demonstrated in Figure 1.8.

Ceramics and ceramic composites

Ceramics include a variety of materials such as oxides, carbides, sulfides, and intermetallic compounds [1]. Bonding present in these materials are mostly ionic, which is significantly stronger than the metallic (covalent) bonding in metals. Furthermore, unlike metals, ceramics do not contain slip planes. This means that while the material is stronger than that of metals, they have very low toughness. Upon fracture, ceramics are extremely brittle. Since they do not contain slip planes, dislocations cannot move and multiply, meaning that they cannot undergo plastic deformation. For this reason, ceramic composites were designed to improve the toughness by combining strong ceramic materials typically with a more ductile matrix phase.

In order to toughen ceramics, a variety of extrinsic mechanisms are used which are shown in Figure 1.7 [1]. Figure 1.9 lists the different types of mechanisms, examples, and corresponding fracture toughness that can be achieved through toughening. With some these mechanisms the fracture toughness can significantly increase going from values of about 3 MPa-√m, to all the way up to 20 MPa-√m, which is the equivalent of some metals.

Toughening Mechanism	Material	Maximum Toughness, $MPa\sqrt{m}$
Fiber reinforced	LAS/SiC	~20
	Glass/C	~20
	SiC/SiC	~20
Whisker reinforced	Al_2O_3/SiC(0.2)	10
	Si_3N_4/SiC(0.2)	14
Ductile network	Al_2O_3/Al(0.2)	12
	B_4C/Al(0.2)	14
	WC/Co(0.2)	20
Transformation toughened	PSZ	18
	TZP	16
	ZTA	10
Microcrack toughened	ZTA	7
	Si_3N_4/SiC	7

Figure 1.9: Toughening mechanisms for ceramics with examples and corresponding fracture toughness values. [7]

With the use of these extrinsic toughening mechanism, the fracture toughness and crack growth resistance of a ceramic can be altered. This allows for the ceramic to transition from low fracture toughness and brittle failure to moderate fracture toughness values with R-curve behavior in some cases. This will allow for further application of ceramics to more industrial needs.

Microcrack toughening

One method of toughening is microcrack toughening.[1, 8] While in most cases for ceramics, adding cracks would not be an effective way of increasing toughness, but optimized microcracking can be beneficial. Microcracks result from the addition of second phase particles to the main ceramic component. These particles can experience residual stress due to thermal

expansion mismatch or transformation. This can happen with either the particle or main component material cracking. With the formation or development of microcracks, there is a corresponding release of strain energy resulting in more compliance and toughness. This mechanism is demonstrated in Figure 1.10.

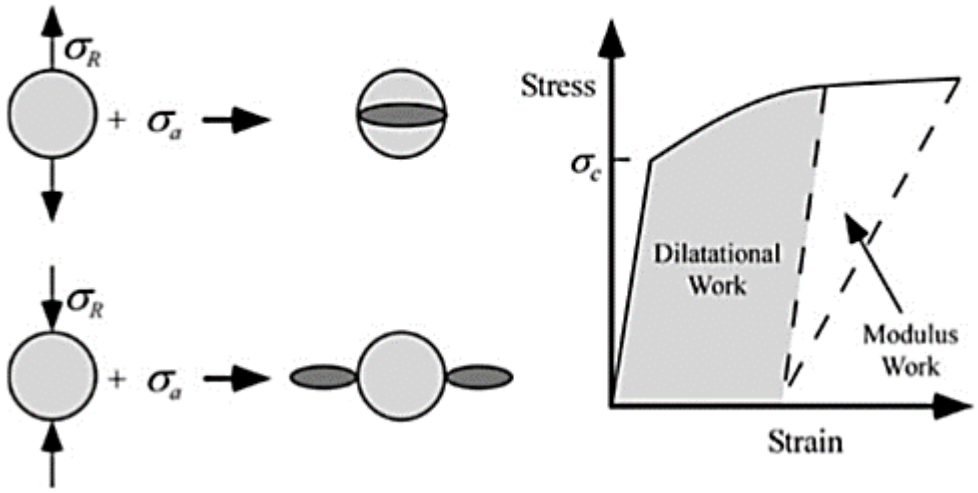

Figure 1.10: Mechanism for microcrack toughening showing the mechanism in (top) or near (bottom) the second-phase particle. With resulting stress-strain curve showing the increased toughness of the composite.[7]

Transformation toughening

Transformation toughening occurs when stress is applied, causing certain ceramics to undergo phase transformation. One example is martensitic transformation commonly seen in zirconium dioxide [1]. This causes the material to experience shear deformation and volume change. This transformation lowers the crack driving force due to energy dissipation, resulting in higher toughness. It is dependent of temperature in which if the temperature goes below the temperature at which the transformation occurs, it will happen spontaneously resulting in no increased toughness. With increasing temperature above the transformation temperature, the stress induced increases with it until too much stress builds up resulting in the mechanism not being effective. The mechanism for this process is demonstrated in Figure 1.11.

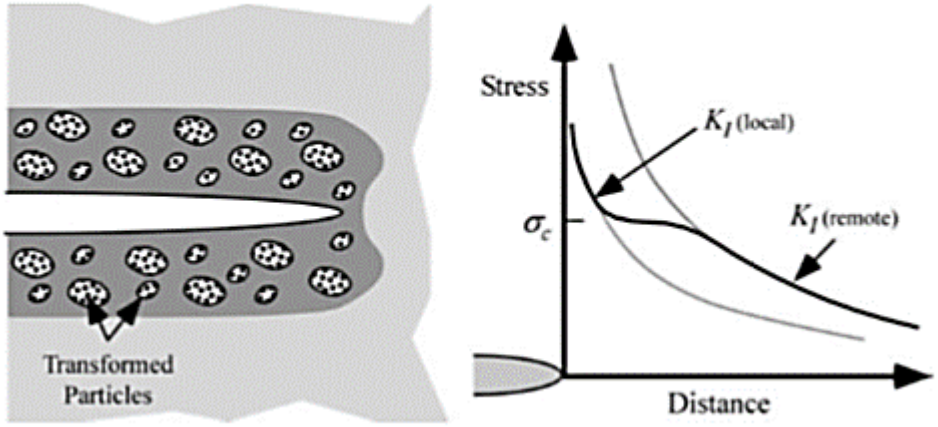

Figure 1.11: Mechanism for transformation toughening with corresponding plot showing how the material experiences a non-linear behavior.[1]

Ductile phase toughening

Ductile phase toughening increases toughness in a variety of ways and as the name states, it is done by adding a ductile phases (metals) [1]. For one, since the phase added is ductile, plastic deformation can now occur, increasing toughness. These particles that are in plane of the crack also undergo ductile rupture causing more plastic deformation. Bridging that occurs at the process zone due to the second phase increases the toughness as well. This mechanism can be seen in Figure 1.12. To further increase the effectiveness of this mechanism, the particle size can be altered by reducing size, resulting in increased toughness [7]. Toughness can additionally be altered by means of temperature. By adjusting the temperature, the flow properties of the metal can be varied. With this mechanism, there is more of a temperature limitation since metals have such lower melting points than that of ceramics.

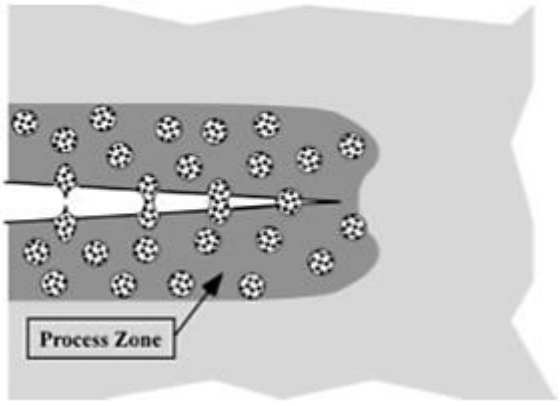

Figure 1.12: Ductile phase toughening due to plastic deformation and bridging at the process zone. [1]

Fiber and whisker toughening

Whisker or fiber toughening produces the highest increases in toughness even with a ceramic second phase [1]. With the addition of brittle interfaces, there are weaker bonding interfaces allowing for a bridging mechanism to occur. Depending on how the whisker or fiber bonds with

the matrix, the ceramic composite will bridge by either fiber/matrix bonds breaking or sliding at the interfaces created with the second phase as shown in figure 1.13. If the bond is strong the crack will grow through the fiber or whisker or if they are not bonded to the matrix, sliding will occur. Both of these mechanism will result in increased toughness. This mechanism is the most beneficial for three important reasons.[9-11]

1. The fibers do no fail at the same time since the strength is subjected to variability.
2. It experiences quasi ductility.
3. Since it is all ceramic, high temperature use is possible.

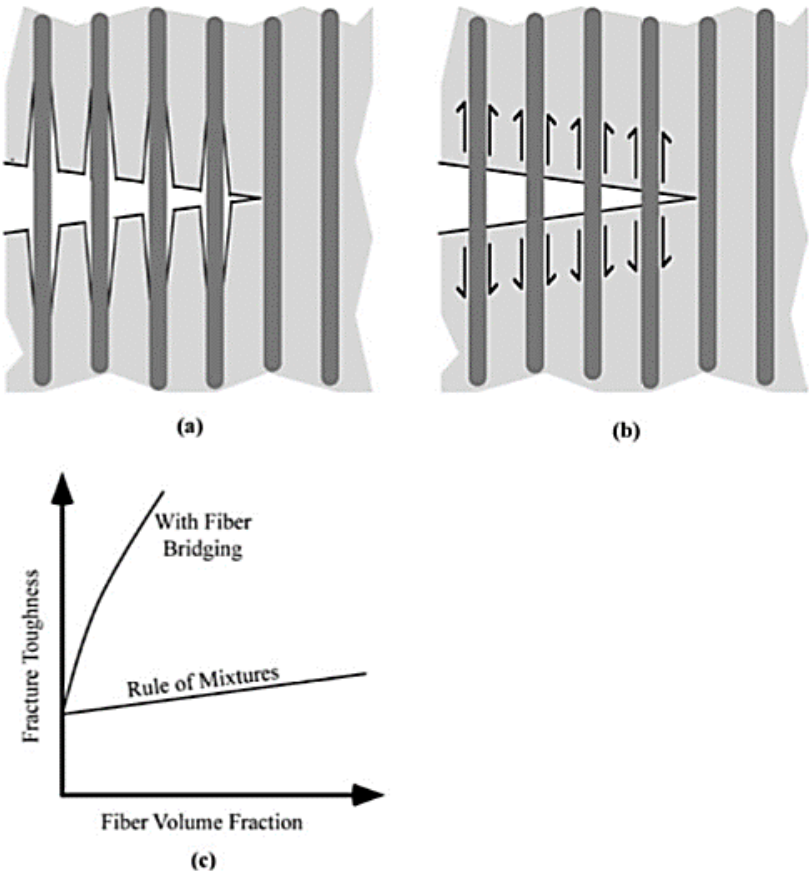

Figure 1.13: (a) Breaking of Fiber/matrix bonding, (b) sliding of interfaces, and (c) graph demonstrating how bridging increases toughness.[1]

1.4.Nacre

As stated in the previous section, different materials have particular ways in which they fracture and ultimately fail. An additional class of materials that can be considered are those found naturally and operate at a systematic level. Engineers have taken clues from nature in designing materials that have enhanced properties. One approach to this is through designing

composite materials and attempting to combine the properties of individual constituents. One common example of this is nacre shown in Figure 1.14(a), which is commonly found in seashells and is known for both is high strength and toughness [12-15].

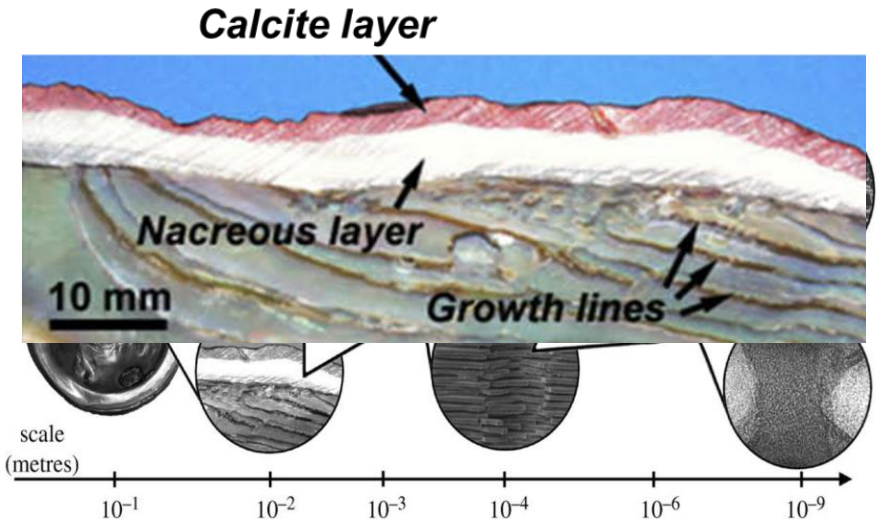

Figure 1.14: (a) Microscopic image of nacre and (b) hierarchical structure of nacre.[12, 16]

The combination of strength and toughness of this material comes from its hierarchical structure as shown in Figure 1.14(b) [15]. Its structure is ordered starting from 10^{-1} meters to all the way down to the nanoscale. The nacreous layer consists of aragonite ($CaCO_3$) plates and organic matrix proteins which are organized together in a brick-&-mortar structure. This layer is able to dissipate stresses by means of inelastic deformation. In between each plates are a complex 30nm thick system which includes layers of organic materials, nanoasperties, and direct mineral connections [15] . The individual plates are composed of nanograins within a three dimensional network of organic material.

The aragonite plates consist of a brick-&-mortar structure, although the structure varies across different species of mollusk as shown in Figure 1.15. Even though the composition does not change, the change in structure effects the mechanical behavior. Out of the six shown (native to different species), the sheet and columnar nacre show the highest combination of strength and toughness. Many studies have shown that not only is their behavior ideal but makes for the perfect models for biomimetic materials [12, 17, 18].

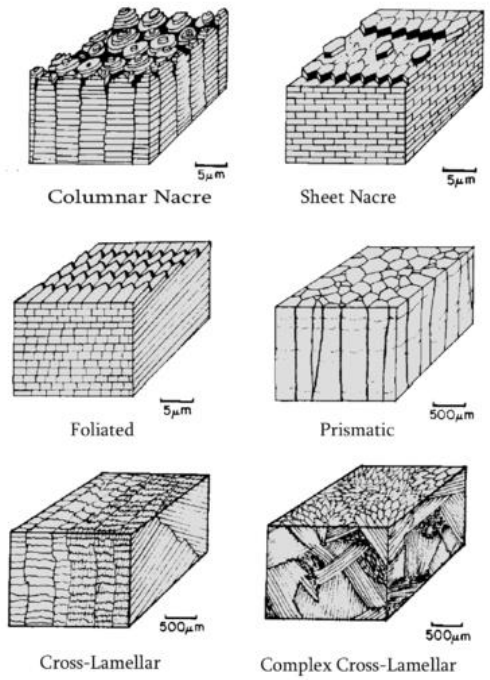

Figure 1.15: Various structures of nacre from different mollusks.[12]

The "brick-&-mortar" structure from the sheet nacre displays interesting mechanical behavior. Nacre has increased toughness due to its elastic-plastic behavior as seen in Figure 1.16, when it is hydrated. This is surprising for a material that consists primarily of a ceramic and can attribute to its high toughness due to the small amount of proteins present between the aragonite plates. This enables sliding of these plates, allowing for deformation and energy dissipation, corresponding to an increase in toughness with the proteins holding the plates in place [12, 13].

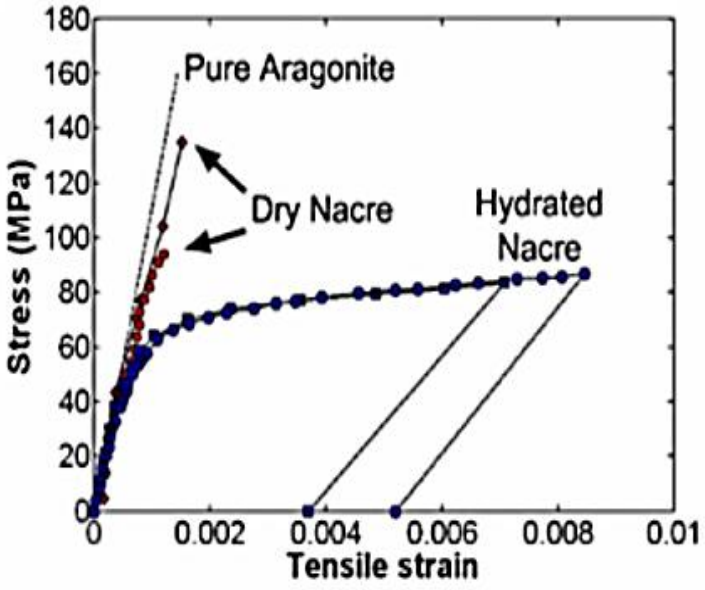

Figure 1.16:Stress-Strain curve for pure aragonite, dry nacre, and hydrated nacre. When hydrated, nacre goes from a linear-elastic behavior to elastic-plastic. [12]

The high fracture toughness achieved through these materials is of great interest to many researchers which will be the focus of this study. This will include the synthesis of nacre-like structures produced with thermal spray, a common manufacturing process used in industry. From there, more detailed information will go into the fracture behavior of these by determining and plotting the J-R curve of the template. The thesis will transition from the standard hybrid composite into modifications of the structure, modifications of the initial epoxy, and replacements that will better the overall toughness and R-curve behavior of the hybrid composite.

2. Background

Using thermal spray, one can produce structures that can behave differently than that of its bulk counterpart. This is achieved through the unique structures produced from this process. In fact, previous work done has shown that with thermal spray, one can produce a coatings as a template to synthesize hybrid composites, that behaves similarly to that of nacre [13]. During this section the varying thermal spray process will be discussed. The section will further discuss thermal spray by describing the structures produced and the resulting properties and applications of each.

2.1. Thermal Spray Process

Thermal spray is a broad term encompassing a group of coating processes used to apply metallic or non-metallic materials [19]. The thermal spray process can be broken down into three types which are flame, electric arc, and plasma spray. These processes either use powder, rod, or wire feedstock to spray the coating. Because of the various materials that can be sprayed and in addition with the various types of spraying, multiple applications are available with this technology. This includes components for gas-turbines, pulp and paper processing, printing rolls, continuous-annealing mill rolls, corrosion protection, biomedical implants, and many other applications [20]. These feedstocks are heated up to either a semi-molten or molten state and solidify upon impact with substrate. Upon the impact and solidification of the “splat”, it bonds to the substrate and continues to be deposited until the coating is formed.

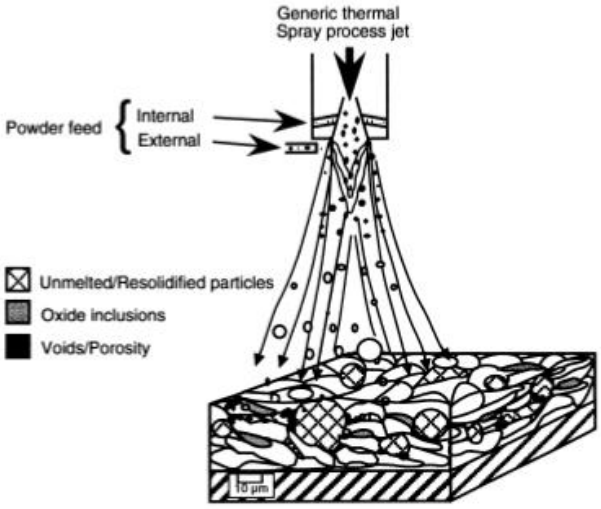

Figure 2.1: Schematic of thermal spay process with resulting coating.[19]

These processes can be used for a variety of materials and applications since any material can be applied as long as it does not decompose upon melting [21]. Thermal spray coatings are also easily taken off or reapplied when damaged, making it easy to service a part. However, the process is based on a line-of-sight design so the coating can only be applied where the torch can "see".

Figure 2.1 shows a typical thermal spray process with the resulting coating sprayed [19]. Feedstock is fed internally or externally from the torch, depositing the coating. Depending on the process and conditions used, the coating will have different artifacts present. These include voids which caused the porosity in the coating, un-melts or re-solidified particles, or oxides from spraying metallic materials.

As mentioned previously, there are three main categories of thermal spray categories [22]. The first one to be discussed is the flame spray processes. The first type of flame spray process uses powder. This process uses a powder feedstock that is flown through an oxyfuel flame that melts the powder and is carried through the flame and air jets. Particle velocity is relatively low compared to other spraying process as shown in table 2.1 which gives the specifics about each spraying process. Due to the lower speed, the bond strength and cohesive strength is weaker causing higher amounts of porosity. The one advantage though, is the higher spray rates associated with it, however, there are high substrate temperatures that occur because of flame impingement. This process is also the same for that of rod feedstock except for which the rod is fed through the back of torch. In addition, the rod feedstock is crushed and fully molten before leaving the torch.

Another type of flame spray is wire flame which involves the melting and afterwards, atomization of the wire feedstock [22]. The molten material is projected towards the substrate at rates similar to that of the previous flame spray process mentioned. Another variation of the process is high velocity oxyfuel process (HVOF). Hydrogen, propane, or propylene is mixed with oxygen to create a combustion jet at high temperatures shown in table 2.1. This combustion process takes place in a high pressured chamber. While HVOF may not deposit as much as powder flame spray, it deposits at much higher velocities causing much better bonding resulting in a very dense coating.

The last type of flame spray process is the detonation torch [22]. This process works by packing the powder feedstock into capsules. These capsules are feed into a barrel and sprayed using oxygen and acetylene. Using a spark to initiate the gas mixture, a controlled explosion occurs, depositing the material. With this process there is combination of high pressure and temperature resulting in a dense and high strength coating. What is also advantageous about this process is the low oxide content present.

The next type of spraying process is the electric arc process [22]. This process uses two wire electrodes with a high current DC power source. This is fed into the torch and the two wires collide with each other causing the tip of wires to melt. When molten, it is atomized and using a stream of air, the particles are sent towards the substrate. The process is energy efficient since all of the input energy used goes to melting the material resulting in high deposition rates. Unlike the flame spray process, there is low substrate temperatures since there is no hot jet of gas propelling towards the substrate.

The last group of thermal processes is plasma arc which is separated into conventional and vacuum plasma [22]. The conventional process is also known as atmospheric plasma spray (APS) which uses plasma temperatures that surpass any other thermal spray process. These

temperatures are acquired by heating up an inert gas using a DC arc. A powder feed stock is used and carried using an inert gas. Due to the high temperatures there is either a high use of cooling or regulation of the spray rate depending on the material and desired conditions. The spray rates vary greatly with this process which is mostly determined by torch design, gases, and materials properties. Vacuum plasma spray (VPS) or low-pressure plasma spraying (LPPS) uses low pressures that alter the dimensions of the plasma plume. With the lower amount of oxygen present, spraying can be done with higher substrate temperatures resulting in denser coatings with better bonding.

Table 1 Comparison of thermal spray processes

Process	Gas flow		Flame or exit plasma temperature		Particle impact velocity		Relative adhesive strength(a)	Cohesive strength	Oxide content, %	Relative process cost(a)	Maximum spray rate		Power		Energy required to melt	
	m³/h	ft³/h	°C	°F	m/s	ft/s					kg/h	lb/h	kW	hp	kW/kg	kW/lb
Flame powder	11	400	2200	4000	30	100	3	Low	6	3	7	15	25–75	34–100	11–22	5–10
Flame wire	71	2500	2800	5000	180	600	4	Medium	4	3	9	20	50–100	70–135	11–22	5–10
High-velocity oxyfuel	28–57	1000–2000	3100	5600	610–1060	2000–3500	8	Very high	0.2	5	14	30	100–270	135–360	22–200	10–90
Detonation gun	11	400	3900	7000	910	3000	8	Very high	0.1	10	1	2	100–270	135–360	220	100
Wire arc	71	2500	5500	10,000	240	800	6	High	0.5–3	1	16	35	4–6	5–8	0.2–0.4	0.1–0.2
Conventional plasma	4.2	150	5500	10,000	240	800	6	High	0.5–1	5	5	10	30–80	40–110	13–22	6–10
High-energy plasma	17–28	600–1000	8300	15,000	240–1220	800–4000	8	Very high	0.1	4	23	50	100–250	135–335	9–13	4–6
Vacuum plasma	8.4	300	8300	15,000	240–610	800–2000	9	Very high	(b)	10	10	24	50–100	70–135	11–22	5–10

(a) 1 (low) to 10 (high). (b) ppm levels. Source: Ref 3

Table 2-1: Table of different spraying processes with details of each. [22]

2.2. Structure of a thermally sprayed material

All thermally sprayed materials are made from a buildup of “splats” which are impacted droplets or particles [23]. These “splats” are typically spherical but can vary slightly in shape depending on spraying parameters and materials as shown in Figure 2.2. They can either be pancake shaped with smoother edges, circular with some grooved edges, or spread out and completely misshapen. Due to the rapid cooling rates, there are grain structures inside the “splat”. Depending on the shape and how molten the “splats” are, the cohesion, porosity, and properties of the coating will vary.

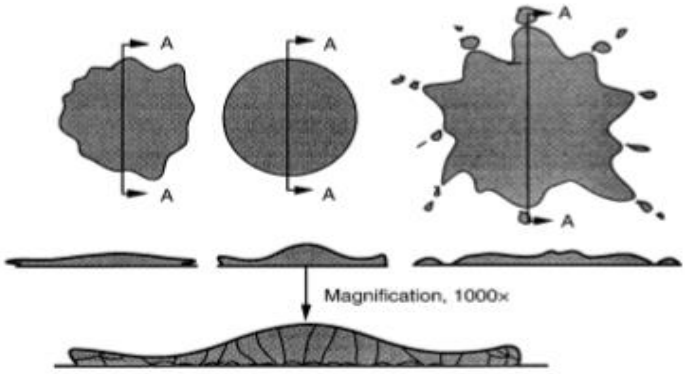

Figure 2.2: Schematic of different splat morphologies and magnified image of a single splat showing grains.[23]

As mentioned previously, depending on how molten the "splats" are, the porosity will be different. Porosity is an important part of a thermally sprayed material and greatly affects the coating's properties [23]. While in some cases, porosity can be quite useful, and in others, it can be undesirable. Porosity results in lower cohesion bonding causing higher wear and corrosion rates. With poor cohesion there is additionally cracking, delamination, or spalling.

Another inclusion in metallic thermally sprayed materials is oxides, which are formed during the process [23]. This occurs during the particle interacting with the atmosphere and high temperatures produced during the process. These oxides produced, have benefits to the coating in the sense that the hardness of the coating increases. While increased hardness can be beneficial, it does lead to a more brittle coating. With oxides in-between the layers, cohesion strength can be weakened.

2.3.Properties of a thermally sprayed material

Because of the various spraying process, materials, and structures resulting from thermal spray, there are a variety of properties that these coatings can have [23]. Thermal spray can produce metallic coatings with high hardness for wear resistance. One of the very popular uses of thermal spray is thermal barrier coatings which are used for thermal insulation. This is achieved by spraying ceramics with porosity and microcracks. The porosity and microcracking not only enhances the insulation, but thermal shock resistance.

Thermal spray also makes for great corrosion protection since it is able to spray corrosion resistant materials [23]. However, interconnected porosity is a common occurrence with these coatings which negate the corrosion benefits. Using a high energy thermal spray process, a dense coating can be produced to resist corrosion. Being able to produce both hard and soft coatings allows for the production of both useful abradables and abrasion-resistant materials. An important feature that comes from porous sprayed ceramics, is that they are able to have a nonlinear response to strain unlike a typical ceramic which experiences brittle failure. This will be further discussed in another section of this chapter.

In addition to great corrosion and mechanical properties, thermally sprayed coatings can have useful electrical properties such as conductivity [23]. This allows them to be used for contacts, electrical connections, heating elements, electromagnetic and radio frequency interference shielding. With thermal spray, a coating can reach bulk conductivity values between 40% to

90%. However, poor conductivity can also be useful for electrically insulating materials by spraying materials such as alumina, alumina/titania, and mullite.

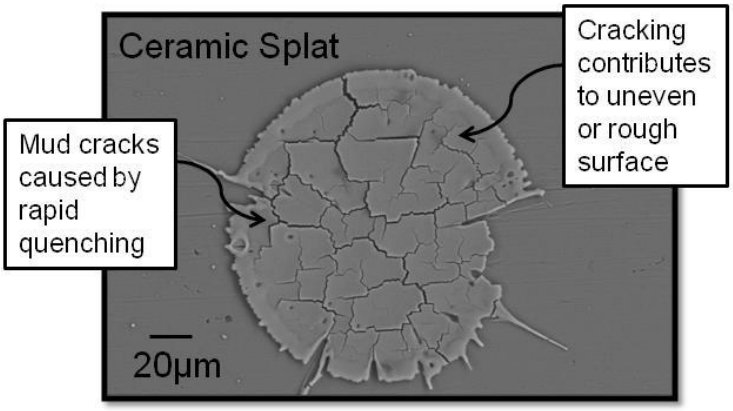

Figure 2.3: SEM micrograph of a "splat" from a ceramic powder thermally sprayed.[24]

The porosity of thermal spray materials makes them useful for medical implantations [23]. Spraying porous titanium on implants allows for cell growth inside the coating making it biocompatible. Allowing it to grow in the inside further secures the implant in place. Bioactive coatings such as hydroxyapatite can be sprayed on implants to support bone growth and eventually be replaced by it. When spraying polymers, their properties are on the same level or greater. This makes them useful for resistance against corrosion, abrasion, and chemical attack.

2.4.Deformation behavior of a thermally sprayed ceramic

Typically, during the spraying of a ceramic powder the "splats" that are deposited contain "mud cracks" causing by rapid quenching during the thermal spray process as seen in Figure 2.3 [24]. Due to this occurrence, there is resulting porosity and cracks throughout the coating and as well as roughness on the surface of the "splat". With the buildup of these defects seen previously in this chapter that they can be quite advantageous to produce properties not seen in the bulk material. One particular effect is that a thermally sprayed ceramic material is able to experience deformation upon failure. While this may make the coating weaker, the material may not experience brittle failure. This occurs since the interface between the layers is weaker than the material itself.

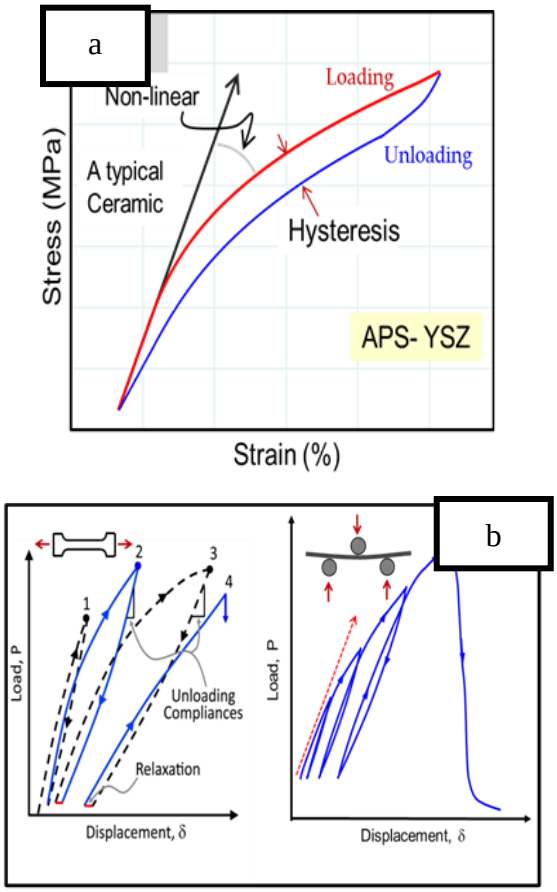

Figure 2.4: Anelasticity shown with (a) bi-layer curvature method with APS-YSZ compared to a typical ceramic showing no anelasticity and (b) mechanical cycling of nacre with tensile loading and 3-point bending of APS-YSZ both showing anelasticity. [24, 25]

Not only do ceramic coatings experience this deformation during failure and non-linear behavior, but also a hysteric response during thermal or mechanical load/unloading cycles [24, 26]. In comparison to a bulk ceramic, they only experience an elastic plastic behavior as shown in Chapter 1. This combination of behavior is known as anelasticity as shown in Figure 2.4 which shows thermal cycling done with the bi-layer curvature method (a) and mechanical loading/unloading with tensile and 3-point bend loading (b). This behavior also seen in nacre is attributed with the defects produced during the thermal spray process.

As mentioned before, this behavior of both anelasticity and deformation comes from the defects present in the ceramic coating. For anelasticity, it roots from the “splat” interfaces and instrasplat cracks while larger cracks and pores affect mechanical properties. The hysteresis portion of anelasticity comes from the frictional sliding of crack faces, the opening/closing of microcracks, and the small pores and voids. These mechanisms are quite substantial since a purely ceramic coating can dissipate energy which is demonstrated in Figure 2.4 [27-32].

3. Statement of problem

High strength and toughness has always been sought out when designing more advanced materials. This is due to the fact that these properties are usually mutually exclusive. An approach to solving this dilemma is by taking a page from nature. An example of this is the design of nacre-like material- a material which is present in sea shells and consists of 95% by volume of aragonite plates and 5% organic matrix. This materials impressive behavior stems from the synergistic effects of the organic matrix binding in between the aragonite plates in addition to its hierarchical structure down to the nanoscale, allowing for a combination of strength and toughness higher than both separate constituents.

Much research has been on trying to synthesize artificial nacre systems. One of such approaches has been the use of thermal spray by synthesizing an assortment of different structures due to the diversity of conditions and available processes that can be used. Thermally sprayed ceramics has been shown to have a novel anelastic behavior which originates from movement of defects within the microstructures with an external mechanical load. These phenomenon introduces a mechanical energy loss, which can be perceived to be supportive from a fracture resistance point of view. While these defects alone may lower the strength and toughness of the material, these artifacts have many benefits for industrial application. One popular application of these porous ceramics is the use of thermal barrier coatings since they are able to thermally insulate, but have thermal shock resistance. A proper combination of spraying processes and conditions can produce a staggered structure which will result in both similarities in structure and properties to that of nacre- a material which is majority consist of ceramic, yet has been known to have great fracture resistance. With the infiltration of an epoxy, the sprayed template further mimics nacre with but higher strength and fracture toughness. These results have been reported in a previous work from our group. Further examination of both the as sprayed and infiltrated template after single edge notch bend testing, showed that there is crack deflection, bridging, branching, and blunting. This signifies that the template and hybrid composite could potentially have a resistance curve behavior which was not discussed in great detail in the earlier work.

The main focus of this thesis will be to develop and validate a method to determine the R-curve behavior of not only these template and hybrid composite but other thermally spray materials (ceramics in particular). These materials are typically weaker than their bulk counterparts and do not undergo much non-linearity upon failure making it difficult to determine such behavior. However, with a combination of equations from ASTM standards for single edge notch bend specimens (E 1820) and the secant method, it is feasible to determine the behavior without the use of imaging or elastic compliance method for the notch extension. By being able to calculate the notch extension without the previous mentioned methods, the limitation of size does not become a factor as well.

While high fracture toughness is indeed essential for many applications, it can be more important that the material has rising R-curve behavior. Rather than having high strength and

toughness, it would be more ideal to have both high fracture toughness along with R-curve behavior. This rising R-curve behavior is of more importance, as it describes the ability of a material to fail under a stable crack growth conditions. From structural application point of view, this behavior is critical. After determining the R-curves for the bio-inspired hybrid composite produced in this study and understanding the behavior for each, enhancements can be made to either the structure or epoxy to achieve both higher toughness and R-curve behavior.

However, there is a limitation with epoxy for applications, which is the low operation temperature. Many applications require temperatures much higher than what the epoxy can withstand (~200˚C), so to overcome this barrier, the introduction of a metal into the template was done. Metals typically have high toughness making it ideal to enhance the template. With thermal spray, such structures are perceivable with a little process modification to adapt co-spraying of metal and ceramic, while maintaining the nacreous-like structures.

With the aforementioned hypothesis, this thesis attempts to define and address the following problems:

1. Does the bio-inspired template and hybrid composite have a resistance curve behavior?
2. Based on the results of 1, can the structure or epoxy be modified to achieve a resistance curve behavior and how would that affect the toughness?
3. Can the replacement of epoxy with metal, have a rising R-curve behavior?
4. How will heat treatment of the ceramic-metallic hybrid composite affect the toughness and R-curve behavior?
5. How will heat treatment with and without vacuum affect how the aluminum bonds and flows with respect to the main ceramic matrix?

4. Experimental

This chapter will describe the different experimental techniques used to process and evaluate the template and hybrid composites studied in this thesis. This includes the thermal spray processes used to design the template and hybrid composites, the infiltration method used for the epoxy used and its modifications, various heat treatment methods, and characterization techniques to determine the mechanical behavior of the template and hybrid composites.

4.1. The thermal spray process

Flame spray process

In order to spray the nacre-like template, a flame spray process was used. The Saint Gobain Rokide® process (Saint Gobain, Worcester, MA) was used which involves using a ceramic rod feedstock that is fed through the back of the torch where it is crushed and fully molten upon spraying. Due to this unique process, an ordered microstructure is produced.

Alumina rod feedstock with a diameter of 6.35mm was procured from Saint Gobain and sprayed at 30 g/min at a 15cm spraying distance. Alumina feed stock was deposited onto aluminum 6061 substrates with dimensions of 152.4 mm x 25.4 mm x 1.6 mm. Substrates were additionally grit blasted mildly before deposition. The torch was moving vertically at 500 mm/s and substrates were rotating on a carousel at 110 RPM. This rotation is essential to get the porosity that is required.

Co-spraying

In order to spray a composite template of alumina and aluminum, both the use of the rod flame spray process and powder flame spray were required to be sprayed simultaneously. The purpose of this co-spray method was to further enhance the toughness and R-curve behavior of the template. Aluminum powder from Metco (54NS-1, d50=66µm) Oerlikon Metco, Westbury, NY) was sprayed with a Terodyn™ torch get the desired volume amount of 34% and 42% of aluminum while still maintaining the ordered alumina structure. The powder flame spray torch and rod flame spray torch both moved vertically at the same speeds. The same substrate, substrate dimensions and preparation, and spraying conditions were used as mentioned in the previous section.

4.2. Removal of template from substrate to make free-standing

In order to preform post-deposition treatments, test templates for 3-point bend testing. and other characterization methods, the template has to be free-standing. To do this the edges were polished using 60 grit paper to remove over spray to weaken bonding between the template and substrate. After grinding, each end of substrate was subjected to cantilever bending to release

template from substrate. Once free standing, template is ready to cut into proper dimensions and receive post-deposition treatments.

4.3.Sample preparation

Once free-standing, samples were sliced into proper dimensions for testing. Samples were sliced to a thickness of 4-6mm and with a length and width of 25.4mm and 1.5mm respectively. Slicing was done with a rotary tool (Wagner, Englewood, NJ) with a diamond disk (Wagner, Englewood, NJ). After post-deposition treatments, templates were polished with up to a 9µm finish using diamond suspension (Buehler Inc., USA).

4.4.Post-deposition treatments

Polymer infiltration

Templates were infiltrated with a 2:1 resin and hardener epoxy (Buehler Inc., USA) under vacuum at 4 mm Hg for 5 minutes. After curing overnight, templates were heat treated in a tube furnace (Barnstead/Thermolyne, Dubuque, IA) at 200ºC for 2 hours to enable cross-linking within the epoxy and strengthen the bonding between the epoxy and the templates' layers.

Polymer modification with acetone

To further enhance the infiltration capabilities of the epoxy system, a technique derived from Loos et al. was used [33]. This involved mixing 10 weight percent acetone with the resin component of the epoxy. Once mixed together, the mixture was then sonicated together for 5 minutes. Following sonication, mixture was placed under vacuum to remove any residual acetone from resin. Standard method for polymer preparation and infiltration was completed after the previous step.

Addition of toughener to epoxy system

In order to give increased toughness to the epoxy and therefore increasing the toughness of the overall template a toughener additive was included into epoxy. 10 weight percent of the toughener Hypro 1300X16 (Emerald Performance Materials, Maple Shade, NJ) was used with it. However due to the higher viscosity of the toughener, 20 weight percent of acetone was included to reduce the viscosity to ensure better infiltrations of the template.

Heat treatments

To understand the effects of temperature on fracture toughness and behavior, templates were heat treated both with (Barnstead/Thermolyne, Dubuque, IA) and without vacuum (General Signal/Lindberg, Evansville, IN) at various temperatures for two hours. Vacuum was chosen to study how oxidation, flowing, bonding of aluminum would change within the template and alter the fracture toughness and R-curve behavior.

4.5.Fracture toughness characterization using 3-point bend for SENB

Templates prepared for testing sliced and polished as stated in the sample preparation method. Following sample polishing samples were notched with a notch length to sample width (a/w) ratio between 0.4-0.6. Notch radius was kept at 80µm or lower using the rotary tool and diamond disc mentioned previously. While mentioned in the introduction that a notch radius of a few microns is recommended, it is not necessary for thermal coatings due to the high defect

density present. Notch length and radius was determined with optical microscopy (Nikon, Epiphot 200, Brighton, MI).

3-Point Bend Setup used was a TIRAtest 26005 (GRC International Inc., USA) using a 200N load cell (Transducer Technologies, Temecula, CA) and a laser to determine displacement of the crosshead. Crosshead speed was set to 0.06 mm/min in order to accurately measure fracture toughness and R-curve behavior from load-displacement curve. Support span was kept constant at 21.06mm for all testing. The fracture toughness equation used was from ASTM standard E1820 that is shown in the next chapter [34]. Data was recorded using a DAQ setup (Omega Engineering, INC., Stamford, CT).

4.6. Microindentation for elastic modulus

To determine modulus of templates, microindentation was done using a Nanotest 600 (Micro Materials Limited, Wrexham, UK) with a 1.6mm WC-Co spherical indenter at 5N max load. Modulus is determined from slope of load-indentation curve produced from test. Hybrid composites were polished down to a 1µm finish for proper contact with indenter. Each template was indented with 30 idents on surface to ensure accurate results by removing any values that fall out of the deviation due to the porosity of the hybrid composites.

4.7. Scanning electron microscopy

To study the misconstrues of each template, each one was mounted and polished using standard metallography practice. Following mounting and polishing, scanning electron microscopy (SEM) was done with a TM3000 tabletop SEM (Hitachi, USA) under backscattered mode at 15 kilovolts. Samples were placed under vacuum at ~1 Torr (Pfeiffer, Nashua, NH). Images were taken 100x, 300x, and 1000x magnification.

4.8. ImageJ analysis for aluminum content

To assess how much aluminum was present in co-sprayed templates, optical microscopy described previously, was used to take five images at 400x. Images were uploaded to ImageJ software (NIH.gov) with the threshold value set to select only the aluminum content. Once the threshold was set a value for percent area converted is calculated which gives the aluminum content present. An average value was calculated from the five individual images taken.

5. Previous work with bio-inspired hybrid composites

Designing a material with both high strength and toughness is a difficult challenge when engineering new materials. In order to overcome this barrier, engineers have taken a page from nature to design materials that can have both. An example of this, as stated previously, is nacre. While consisting of 95% aragonite plates, it experiences anelasticity by the platelets sliding against each other. This is further strengthen with the 5% by volume of organic polymer present in between the platelets. This combination of materials allows for both reasonable values of strength and toughness.

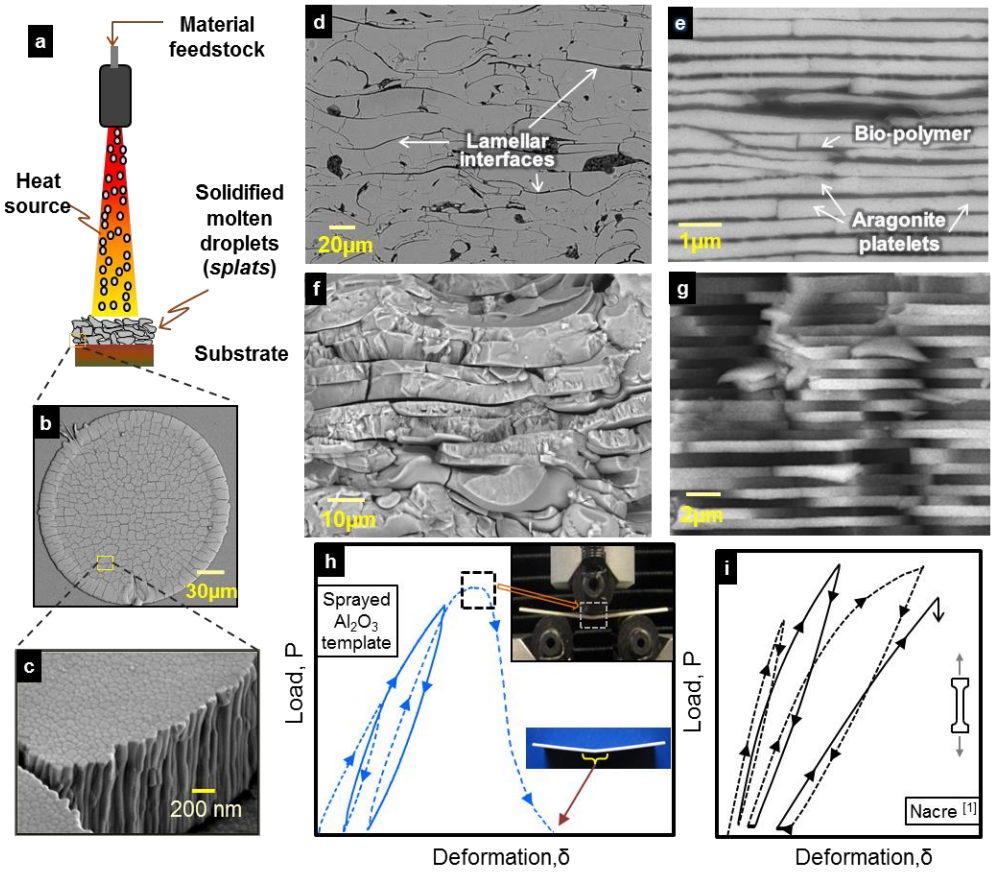

Figure 5.1: (a) thermal spray process (b & c) image of splat with "mud-cracking" showing nanograins inside splats. (d and e) comparison of brick wall structure with nacre. (f and g) fracture surface of brick wall structure and nacre. (h and i) Mechanical behavior of both brick wall structure and nacre.[13]

Multiple works have previously been done with synthesizing nacre-like hybrid composites. Work done by Deville, et al designed an alumina nacre-like structure with ice templating [35]. A

liquid solution is present in between the layers to have a similar organic matrix to that of nacre. The resulting structure presented a combination of both high strength and toughness values of 470 MPa and 6.2 MPa-√m at room temperature. Furthermore, toughening mechanisms such as crack deflection, multiple cracking, and crack bridging and branching were present, which is similar to that of nacre.

Other work done by Ritchie, et al. used freeze casting with alumina, creating a layered porous scaffold [14]. The scaffold was then infiltrated with PMMA to simulate the organic matrix of nacre. A brick-and-mortar hybrid composite was also designed through pressing of the lamellar materials with sintering, resulting in a higher ceramic content (80% vol.). The strength of the materials was lower than bulk alumina, but higher in fracture toughness. The study also concluded that the brick-and-mortar structure had higher values than that of the lamellar structure. Structures displayed similar toughening mechanisms to that of Deville et al. Using thermal spray and epoxy infiltration, a brick-and-mortar hybrid composite was created to mimic the properties of nacre.

5.1. Thermally sprayed template and hybrid composite

Using the Saint Gobain Rokide® process an alumina rod feedstock is fed through the torch until it is fully molten, forming molten droplets, which successively deposit on substrate and form splats [13]. Each “splat” produced results in a rough surface and nanometer scale of columnar grains produced due from the flow of the material upon impact. This results in a highly ordered structure show in Figure 5.1(d) which can be described as a brick-wall structure. Instead of containing mostly globular pores such as in a typical thermally sprayed coating, this structure has interlamellar pores and as well as intersplat interfaces and cracks. Compared to nacre in Figure 5.1(e), there are similarities in structure except for the size of the layers and the nacre structure being more ordered. The nacre structure in addition, contains the biopolymer mentioned in the introduction section. Observing the fracture surfaces of each material in Figure 5.1(f) and 5.1(g), it is seen again how similar in structure they appear.

In addition to similar structure, the template has similar mechanical properties to that of nacre as shown in Figures 5.1(h) and 5.1(i) [13]. 5.1(h) shows the mechanical response of the brick-wall template under loading/unloading with 3-point bend. During this, the template exhibits hysteresis and non-linearity even though it is only ceramic. This behavior occurs due to the layered nature of the template structure. With this brick-wall structure, the rough layers are sliding against each other allowing energy to be dissipated, which is very limited with the disordered structure. In Figure 5.1(i) shows the load-displacement behavior of nacre under tensile loading. Intermediate loading and unloading was conducted on the nacre specimen. The combination of ceramic plates and organic matrix in nacre allows for the dissipation of energy from the sliding and the ceramic plates which is reinforced with polymer stretching to enhance the strength and toughness.

In order to have the template possess the same design of nacre, epoxy was infiltrated into the template [13]. To assess the effects of the polymer on the mechanical behavior of the hybrid composite, both flexural strength and fracture toughness was tested with 3-point bend. In addition, to show the benefits of the brick-wall template, a standard thermally sprayed coating with alumina feedstock was produced with the powder flame spray process. Following spraying, the disordered template was infiltrated with epoxy as well. Figure 5.2 shows the microstructures and fracture surface of each template infiltrated with epoxy. The disordered template (a & c) has only globular pores but higher amounts of epoxy compared to the ordered structure (b, d, & e).

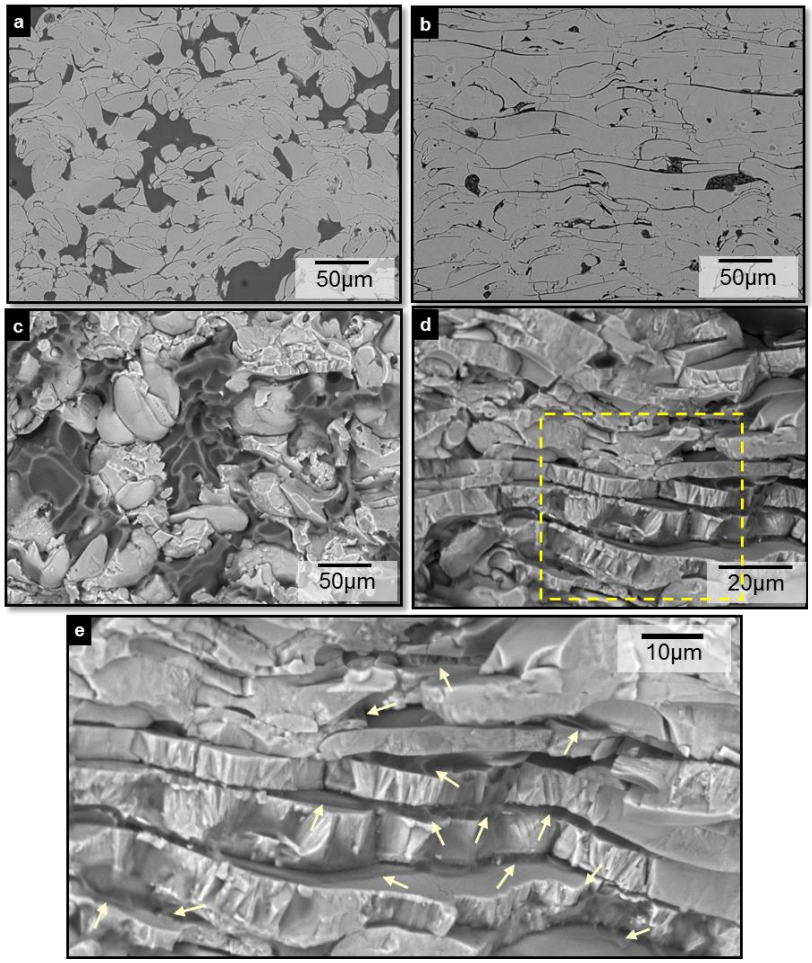

Figure 5.2: (a & c) Microstructure and fracture surface of disordered template, (b & d) microstructure and fracture surface of ordered template, and (e) higher magnification image of ordered template showing epoxy present in between layers.

Figure 5.3 shows the flexural strength (a) and fracture toughness (b) for the disordered and ordered template, with and without epoxy [13]. When comparing the templates in the as sprayed condition, the ordered template has both higher flexural strength and fracture toughness. The higher strength and toughness stems from the ordered structure containing very few globular pores, strengthening the structure. With the brick-wall structure the effect of interlayer sliding serves as an additional strengthening and toughening mechanism.

Both templates receive increased values in strength and toughness when the epoxy is infiltrated [13]. However, the ordered structure exhibits a much more significant increase in values once the epoxy is infiltrated. The brick-&-mortar hybrid composite increases in strength and toughness by around 800% and 600% respectively. The disordered structure's strength and toughness only increases by 400% and 300%. These significant differences with epoxy infiltrating in the templates are attributed with the templates' structures. Since the disordered structure has only globular pores the epoxy does not effectively enhance the properties of the template even though more is present with this structure. The significant increase from the

ordered structure comes from its brick-&-mortar design that allows for great synergistic effects. Since the epoxy infiltrates in between the layers as seen in Figure 5.1(e), it bonds the layers together further increasing the energy dissipation from interlayer sliding. What is also important to note is that the brick-&-mortar template has strength higher then nacre and toughness that is in the same range.

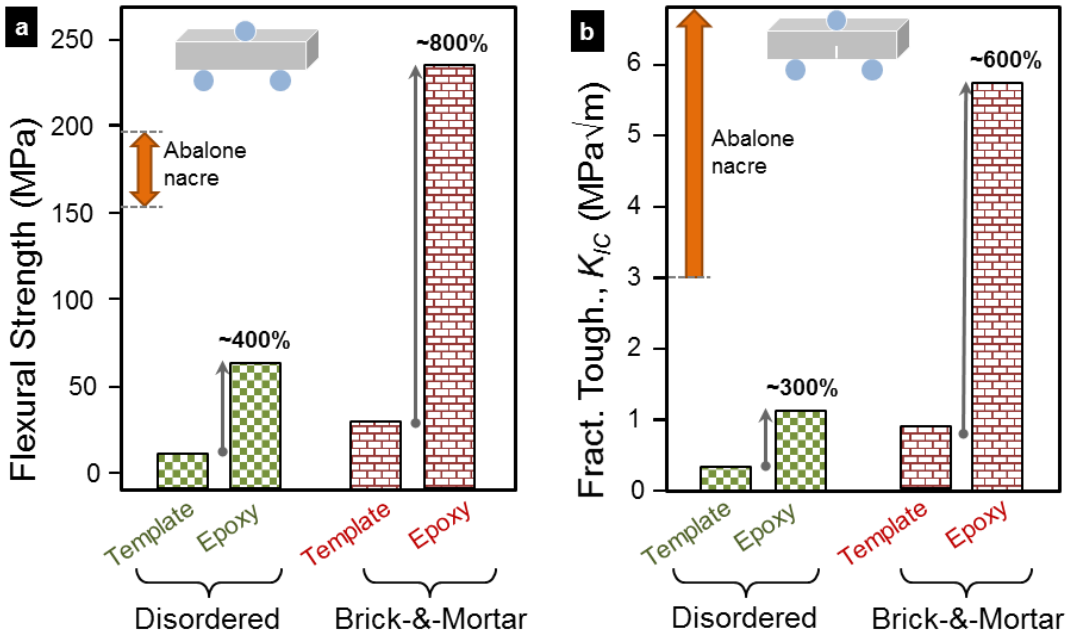

Figure 5.3: (a) Flexural strength and (b) fracture toughness of bio-inspired hybrid composite and traditional thermally sprayed coating compared to nacre.[13]

Figure 5.4(a-d) gives a further observation into the behavior of the hybrid composite upon fracture [13]. Using SEM on a fractured sample the cracks path can be seen and studied. (a) Shows the crack path of the brick-&-mortar hybrid composite after fracture toughness testing. From here it is observed that the extrinsic toughening mechanisms, layer/interface sliding and crack meandering (crack does not propagate straight) are observed. In addition, this interfacial sliding has been reported previously in this thesis which results in the anelastic behavior of these sprayed ceramics. Figure 5.4(b & c) shows a closer examination at the crack and besides the previous mentioned toughening mechanism, the crack dissipated energy occasionally by branching and blunting. In (d) it's clearly shown the epoxy is stretching as it holds the layers in place. Figure 5.4(e) shows the stress strain curves for bulk alumina, nacre, and the ordered template with and without epoxy. When the epoxy is added it can withstand both higher stresses and strains than that of nacre. The bulk alumina is there as a reference point which shows higher stresses but less strain than of the thermally sprayed alumina with epoxy.

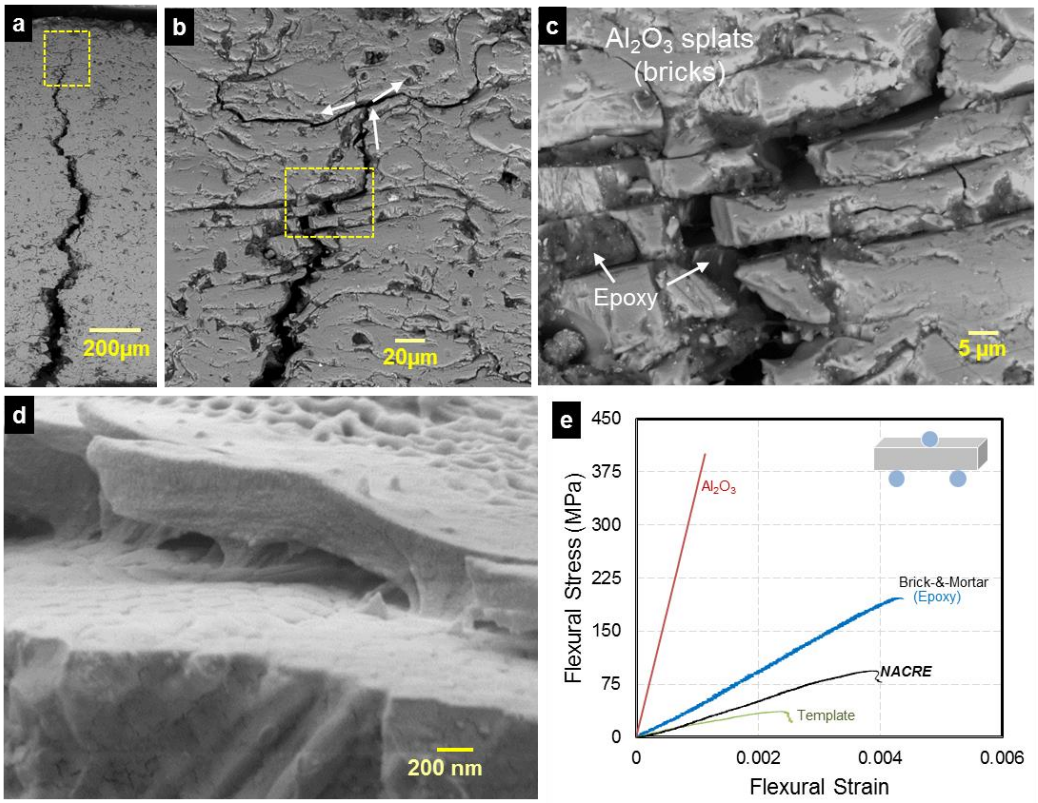

Figure 5.4: (a-d) SEM images of crack propagation of "brick-&-mortar" hybrid composite showing crack bridging, blunting, and plate sliding, and as well showing epoxy stretch during testing. (e) Stress vs. strain curves for as sprayed template, nacre, "brick-&-mortar" structure and bulk alumina.[13]

Lastly, Figure 5.5 shows a plot of fracture toughness vs. flexural strength for the templates and hybrid composites shown in this study [13]. Bulk alumina, and other literature on designing nacre-like systems. At the time of the work, the brick-and-mortar hybrid composite has one of the highest combinations of strength and toughness.

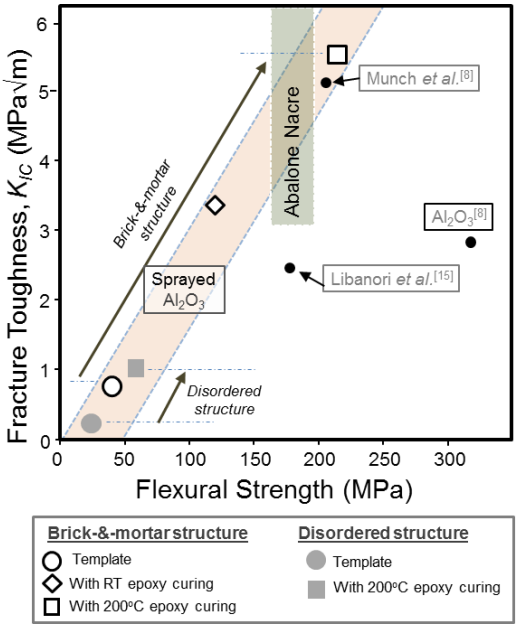

Figure 5.5: Fracture toughness vs. Flexural strength plot of the templates and hybrid composites tested in this study in addition to nacre, bulk and thermally sprayed alumina, and other literature designing bio-inspired hybrid composites.[13]

5.2. Conclusions

The results from this study has concluded that a successful thermal spray template and hybrid composite has been created that resembles both the structure and mechanical behavior to that of nacre. The as sprayed template and hybrid composite appear to exhibit two principle extrinsic toughening mechanisms, (1) interlayer sliding during loading and unloading, and (2) crack meandering, which is similar to the mechanism involved with nacre. This unique ability (sliding) allows for a purely ceramic material to experience hysteresis and anelasticity. The strength and toughness of this template can be significantly enhanced when epoxy is infiltrated into the template and has similar synergistic effects that are present in nacre. The study also concluded that this ordered structure makes a difference in the strength and toughness as well as how much and how effective epoxy infiltration can enhance the template. Based on how the material mechanically responds under an applied load and the extrinsic toughening mechanisms involved during crack propagation, the template and hybrid composite may have a rising R-curve behavior meaning that the material requires additional energy for the crack to propagate. The next chapter will discuss how a method was developed to determine this using 3-point bend and then tested against literature to confirm the accuracy of this method. Following the confirmation of the method, testing for the R-curve behavior of these two were conducted.

6. Determination of J-R curves using 3-point bend technique and secant method

Determining the energy release rate vs. notch extension plots (J-R) will have great benefits in understanding how the materials act upon fracture. A material can have high fracture toughness but if it has no R-curve behavior it will experience brittle failure right when the crack initiates. A challenge with the materials is the size at which we can process and the low amount of deformation the coatings experience. In order to determine these plots, equations used from ASTM E 1820 standards and as well as the secant method to determine notch extension without the use of an optical microscope or unloading/loading of the sample was used.

6.1. Method to calculate J-R plot

To determine the fracture toughness and energy release rates, equations from the ASTM standards for measuring fracture toughness (E 1820) was used. Testing was done using a single edge notch bend so the proper equations were chosen for that method. Before the previous values stated can be calculated, the notch length for each measurement needs to determined. Typically, this is calculated either using an optical microscope to directly measure the crack growth or using the elastic compliance method. The latter method consists of loading/unloading the sample in the non-linear portion of the load-displacement curve and using the inverse of the slope of such sequence to calculate the crack extension as demonstrated in Figure 6.1.

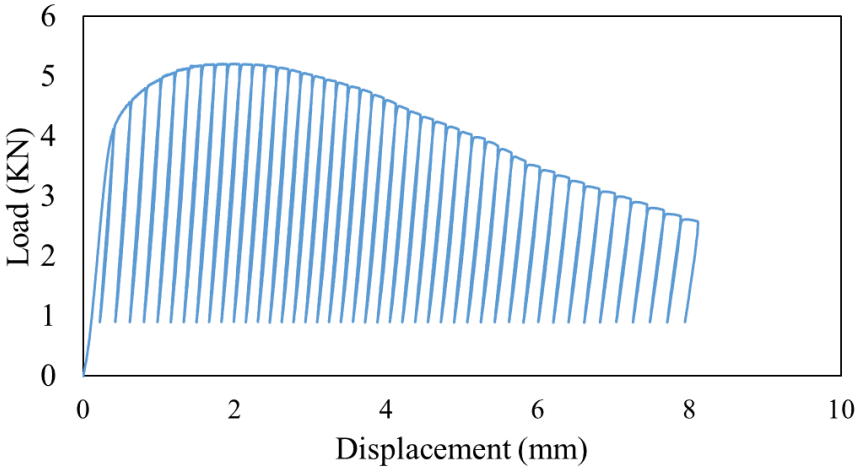

Figure 6.1: Material tested using the elastic compliance method were notch extension is calculated from slope.

However, because of the size, material, and low deformation of the samples, it is not possible to perform such loading-unloading sequences. Therefore, the crack extensions were estimated

using a method, similar to the compliance method, which involved the measurement of mechanical compliance of the ceramic specimens via secant slope of various points on load displacement curve. This method assumes that upon a full unloading at any given point of the non-linear portion, the residual strain would be minimal. This methodology has been adapted in many studies, particularly those which involve small dimensions ceramic test specimens [35].

$$a_n = a_{n-1} + \frac{W-a_{n-1}}{2} * \frac{C_n-C_{n-1}}{C_n} \qquad (5.1)$$

$$K_i = \left[\frac{P_i * S}{(B*B_n)^{1/2} * W^{3/2}}\right] * f(a_i/W) \qquad (5.2)$$

$$f(a_i/W) = 3(a_i/W)^{1/2} * \frac{\left[1.99-(a_i/W)(1-a_i/W)*\left(2-3.93(a_i/W)+2.7(a_i/W)^2\right)\right]}{2(1+2a_i/W)(1-a_i/W)^{3/2}} \qquad (5.3)$$

Equation 5.1 is gives the current crack length at a given point on the load-displacement curve where a_n is the notch lengh, W is the thickness, C is the inverse of the slope at the taken point, and a being the crack length [34]. Since the crack length is calculated, the rest of the values can be done. Fracture toughness is calculated using equation 5.2. K_i is fracture toughness, P_i is the force, S is the support span, B is the width of the sample, B_n is the net specimen thickness, W is the thickness and f(a/W) is a function of the notch thickness/total thickness ratio. The equation for calculating this function is shown in equation 5.3 [34].

$$J = J_{el} + J_{pl} \qquad (5.4)$$

$$J_{el} = \frac{(K_i)^2(1-\nu^2)}{E} \qquad (5.5)$$

$$J_{pl} = \left[J_{pl(i-1)} + \left(\frac{2}{b_{(i-1)}}\right)\left(\frac{A_{pl(i)}-A_{pl(i-1)}}{B_N}\right)\right] * \left[1 - \frac{a_i-a_{(a-1)}}{b_{(i-1)}}\right] \qquad (5.6)$$

Once fracture toughness has been calculated, the energy release rate can be calculated which is broken into two parts as seen in equation 5.4 where J_{el} is the elastic portion of the energy release rate and J_{pl} is the plastic portion of it [34]. The elastic portion is shown in equation 5.5 where ν is poisson's ratio and E is the elastic modulus. Shown in equation 5.6 is the plastic portion where $b_{(i-1)}$ is the remaining un-notched thickness and A_{pl} is the area measured under the load displacement curve between two points. The trapezoidal method is used to calculate the area in 5.6. Using all these equations at various points throughout the load-displacement curve allows for chart plotting the energy release rate vs. the notch extension. Methods describe to determine notch extension and area under the curve are demonstrated in Figure 6.2.

In order to calculate the equations and plot the data, a program using MatLab™ was created using the above mentioned equations and following procedure that the program ran:

1. The output data file from fracture toughness test is chosen and uploaded into the program
2. When uploaded, the file is tared and plotted correctly as a load-displacement curve
3. Dimensions of specimen, notch size, support span size, possion's ratio, number of points to take, and transition displacement - a point on the load-displacement curve where the curve transitions from linear to non-linear behavior.
4. Takes points based on the amount of points chosen to get the notch extension for each one that are after the transition point.

5. Converts to stress-strain to calculate modulus by subtracting notch depth from total width.
6. Calculates fracture toughness at each point taken.
7. Calculates the elastic portion of the energy release rate
8. Calculates area under the load-displacement curve.
9. Calculates plastic portion of energy release rate.
10. Sums the elastic and plastic part and plots against notch extension as well as fracture toughness (K_i and K_j) vs. notch extension.

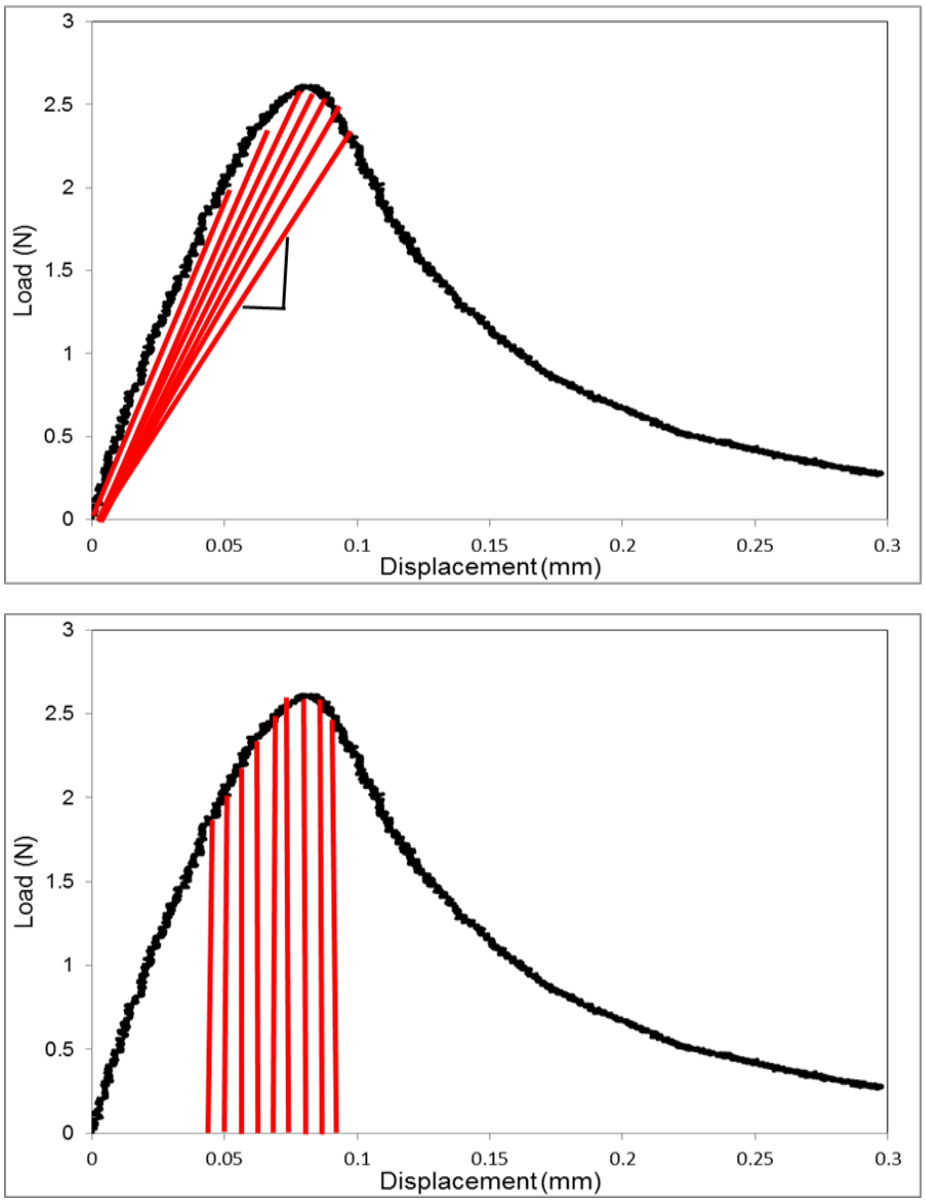

Figure 6.2: depiction of how (a) slope is calculate using secant method (b) how area is calculated under the curve.

6.2Validation of method

In order to validate the methods stated above with the setup, samples were tested that are similar to literature materials and values. This was done by using Damani, et al. work with plasma sprayed alumina with porosities around 13% and 14% [36, 37]. Two different runs were sprayed with the second run rotated after a number of passes to get uniform thickness due to the amount of cooling used. Once material was sprayed, it was removed from substrate by using an acid solution of a 3:1 ratio of hydrochloric (Stony Brook University, Stony Brook, NY) and nitric acid (Sigma Aldrich, Milwaukee, WI). The second run delaminated without acid. Once freestanding, sample were sized to the dimensions of 3mm x 4mm x 27mm similar to the literature using procedures shown in experimental section.

Notching procedures are the same as shown in the experimental except for an additional step to further sharpen the notch down to a 100µm diameter as shown in the literature. This is done with a razor blade using a diamond paste. Figure 6.3 shows an image of a sample prepared (a) and an optical image showing the notch size (b). The notch diameter shown is 106.48µm making it close to what the literature has.

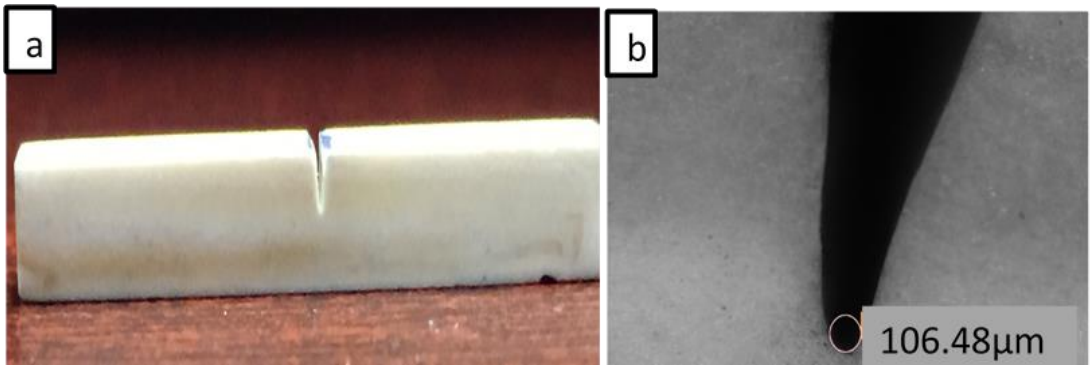

Figure 6.3: (a) Picture of a sample used to validate method and (b) optical image of notch with notch dimeter of sample.

Sample was tested using 3-point method describe in experimental but instead using a crosshead speed of 0.5 mm/min. Once tested, the load-displacement curve is placed into the program mentioned in the previous section. Results concluded that both the notch extension and fracture toughness values are accurate as shown in Figure 6.4 which shows the values calculated with the method and the values obtained from the literature. The slight differences in both the notch extension and fracture toughness stems from that a different method for testing was done and as well as a larger sample was prepared.

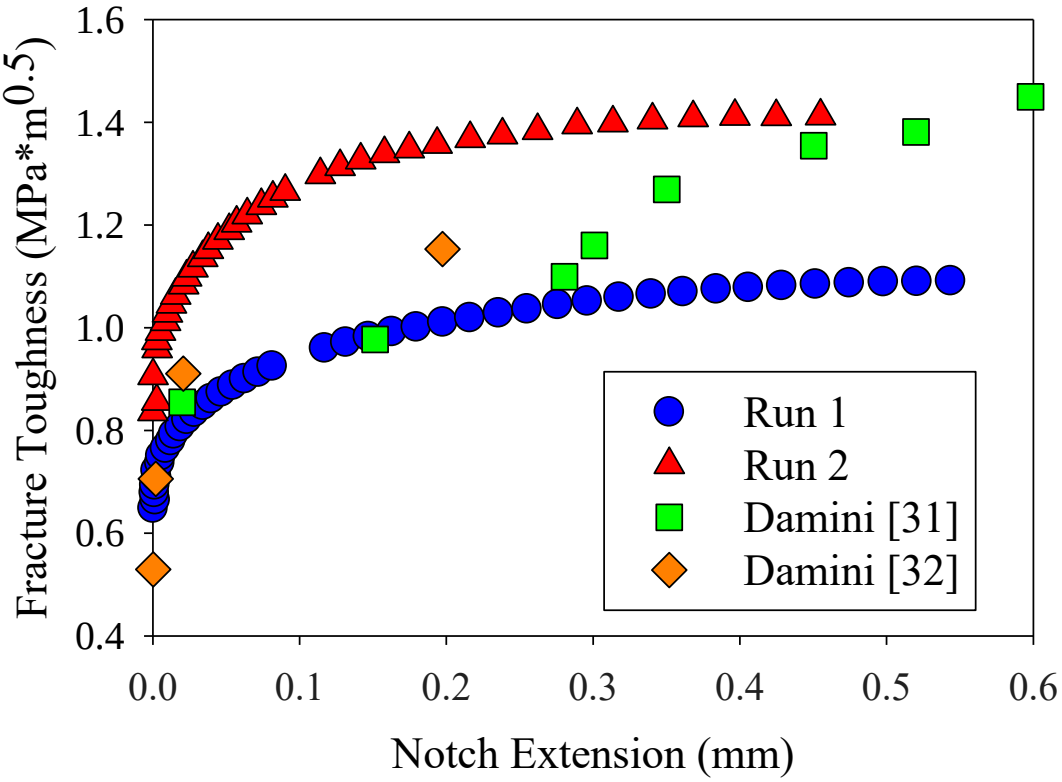

Figure 6.4: Literature values of fracture toughness vs. notch extension compared to values calculated with the methods with log fits. Note that values calculated with the method are similar to literature. The slight differences are due to the larger sample sizes used in the literature and the size of the initial crack length.

6.3 Conclusions

Using equations from the ASTM and the secant method from Deville, et al., accurate measurements for fracture toughness and notch extension have been calculated. Knowing that the fracture toughness values are accurate, the values determined for the energy release rates will be valid as well. This is important since with the method, R-curve behavior for any material, regardless of toughness and size, can be determined. This is also significant since further understanding of the fracture behavior of coatings processed can be done. Previous work done with designing a bio-inspired hybrid composite with thermal spray showed evidence of rising R-curve of both ceramic template with and without epoxy. This will be studied in the next chapter of this thesis.

7. Fracture behavior of bio-inspired template and hybrid composite

The study of artificial bio-inspired hybrid composites has been widely studied using different methods. A previous study, discussed in the earlier section, designed a bio-inspired hybrid composite using the thermal spray process and infiltrating it with a two-part epoxy. Results showed a substantial benefit from the introduction of the epoxy, increasing its fracture toughness up to 600%. SEM images from fractured sample showed the layered splats sliding to dissipate energy. Imaging from SEM additionally show that bridging, branching, and blunting of the crack further showing energy dissipation. The paper concluded that due to these effects, rising R-curve behavior could be present in the template and hybrid composite. Using the methods from Chapter 6, a similar template and hybrid composite will be tested to determine R-curve behavior. This chapter will also focus on how alternating the epoxy or template to modify fracture toughness and R-curve behavior.

7.1 Fracture behavior of as sprayed and epoxy infiltrated templates

Template was processed with standard spraying parameters discussed in experimental using the Rokide® Spraying Process. Figure 7.1 shows the microstructure of the template at 300x (a) and 1000x (b) magnification. From the Figure it can be seen that template has an ordered brick structure with interlamellar pores, intersplat interfaces and cracks, and as well as globular pores. It is important to note that the template microstructure was designed to have reduced globular

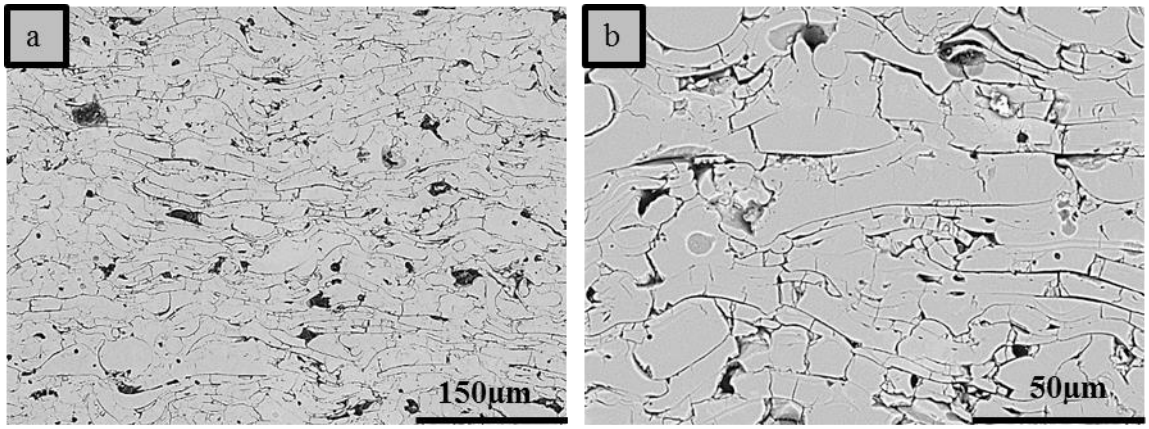

Figure 7.1: Microstructure images of bio-inspired template at (a) 300x and (b) 1000x.

pores and to have more of a layered structure [13].

Fracture toughness of the template was tested using the 3-Point Bend Method, and it was shown that there was a significant increase in toughness when epoxy was infiltrated into the template as reported in Figure 7.2(a). The fracture toughness of the as sprayed template reported only a fracture toughness of 0.79 MPa-√m while the template infiltrated with epoxy reported a value of 3.97 MPa-√m which is about a five-fold increase in toughness. 7.2(b) shows the corresponding load-displacements for tested template and hybrid composite. The as sprayed template may show a lower critical load but displays some non-linearity upon failure. The infiltrated template on the other hand shows a higher critical load but brittle failure.

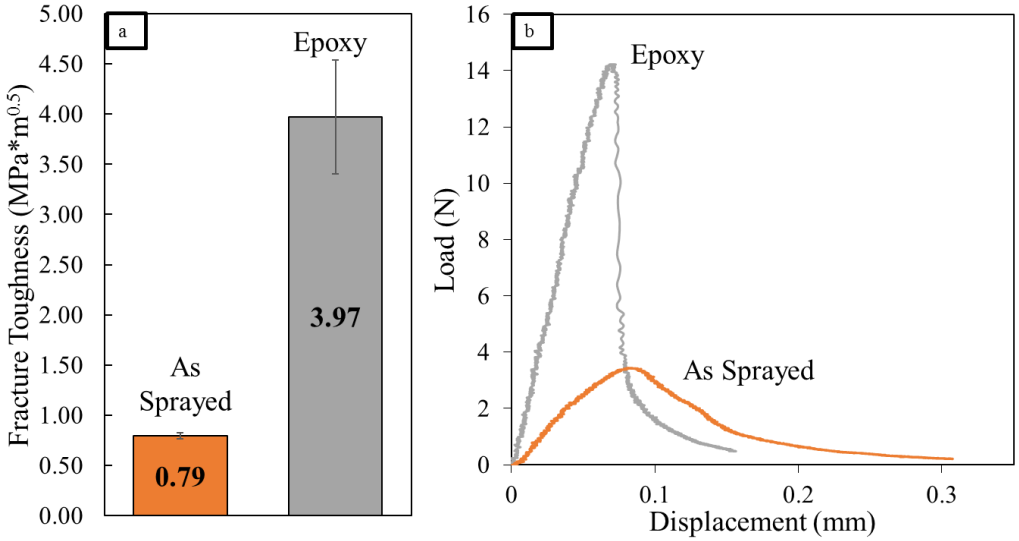

Figure 7.2: (a) Fracture toughness values and (b) load-displacement curves corresponding to 3-Point Bend testing done. While epoxy template shows higher fracture toughness, the as sprayed template has a more graceful failure.

Using the load-displacement curves from the fracture toughness testing, a plot of the energy release rate against the notch extension is created as shown in Figure 7.3. The as sprayed template showed low energy release rates values but demonstrated a rising R-curve behavior seen in Figure 7.3. This behavior corresponds with the template's load-displacement curve, which showed a low critical load, but with a "graceful" failure.

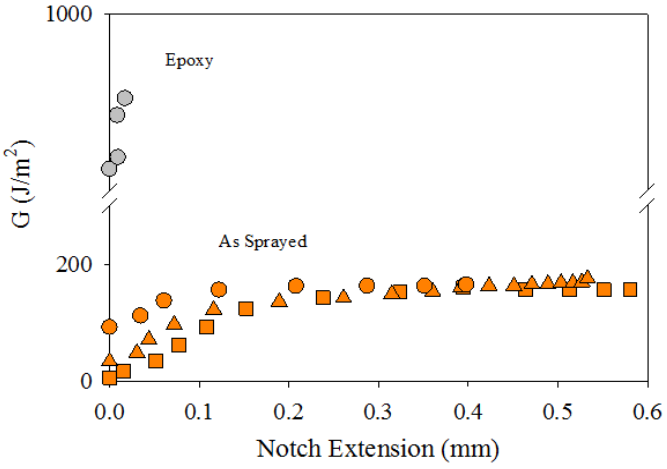

Figure 7.3: J-R plots for the as sprayed and epoxy infiltrated template. The as sprayed shows low release rate values but crack growth stability while the epoxy infiltrated template has considerably higher release rates but no stable crack growth

The epoxy infiltrated template presents opposite behavior that of the as sprayed template. While this template displays significantly higher energy release rates and fracture, it has flat R-curve behavior. This in turn shows that the hybrid composite shows no crack growth. Examining the load-displacement curve, it is observed that the results from the J-R plot correlate to it by the hybrid composite exhibiting brittle failure.

The behavior of these template and hybrid composite comes not only from the material's properties itself, but how the material was processed. Since it was designed with a well ordered and layered structure the as sprayed template exhibits rising R-curve behavior unlike its bulk counterpart that displays brittle failure. The as sprayed template has the ability to dissipate the energy primarily from two extrinsic toughening mechanism- the sliding of the layers/interfaces and crack meandering following least resistance path in the microstructure. This may result in crack blunting in some occasion. These toughening mechanisms have been previously seen with work other bio-inspired hybrid composites [14]. This can be seen from the load-displacement and J-R curves. However, due to the porosity of the template, there is significant reduction in fracture toughness compared to bulk.

The epoxy infiltrated template may experience brittle failure, but presents higher fracture toughness then that of bulk alumina. This results from the epoxy being infiltrated into the template and then being heat treated causes cross linking of the polymer. This allows for better load transfer, but with deficit of the extrinsic toughening mechanisms mentioned previously. Since the energy required crack initiation is much higher, extrinsic toughening mechanisms do not dissipate enough energy, and flat R-curve behavior occurs. Based on work done by Sen and Buehlar, the brick-and-mortar hybrid composite created here does not have enough of a hierarchical complexity to that of nacre [38]. According to this work, this hybrid composite only has a two-hierarchy system.

7.2 Effect of polymer modification on fracture behavior

In order to enhance fracture toughness, energy release rates, and R-curve behavior, the epoxy was subjected to different modifications and additives. These were acetone and the toughener explained in the experimental section. Figure 7.4 shows the fracture toughness results and the load-displacement curves. For comparison, the results from the epoxy were added to Figure 7.4 as well. Compared to the standard epoxy, the additives produced lower results. The addition of acetone alone lowered the fracture toughness slightly to 3.54 MPa-√m but still resulted in brittle failure.

Previous work done by Dr. Flynn reported an average fracture toughness value of 5.7 MPa-√m with toughener used in this study[24]. Subsequent results here do not reflect this due to the use of a new epoxy that was not used in her study. The next hybrid composite used a combination of acetone and a toughener which further lowered the fracture toughness down to 2.86 MPa-√m. However, unlike the other hybrid composites, this one shows some "graceful" failure upon crack initiation. Although it may not be able to withstand loads as high as the epoxy with or without acetone, it behaves similarly as the as sprayed template in terms of failure.

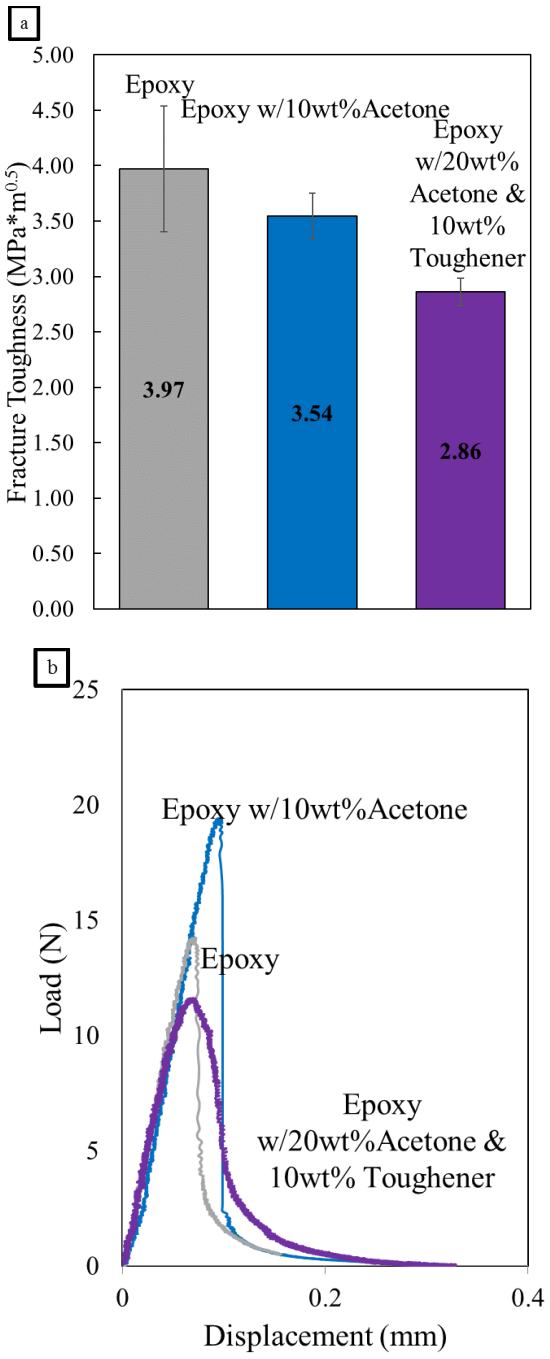

Figure 7.4:(a) Fracture toughness values and (b) load-displacement curves of template with epoxy and epoxy with acetone and/or toughener

Figure 7.5 shows the corresponding J-R curves for each hybrid composite with the addition of the standard epoxy hybrid composite. All the specimens for this figure show higher G compared to the as-sprayed standard specimen (not shown here). The hybrid composite with the epoxy and acetone mixture show slightly higher energy release rates but like the standard epoxy hybrid composite, the extrinsic toughening mechanisms are inhibited. This also signifies that it demonstrates flat R-curve behavior. When there is a combination of the acetone and toughener

with the epoxy, there is a rising R-curve behavior with values higher than that of the as sprayed template in Figure 7.3. However, the R-curve behavior for this modified epoxy, does not have as much defined rising R-curve behavior compared to the as sprayed template.

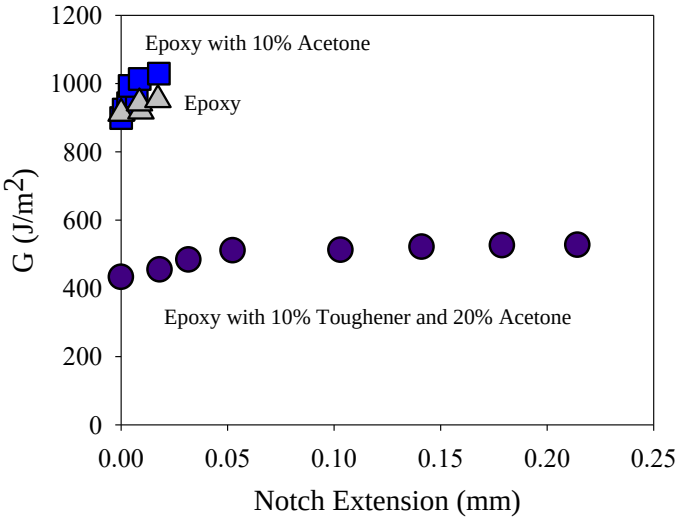

Figure 7.5: J-R Curves for Epoxy, epoxy with acetone, and epoxy with acetone and toughener.

With the addition of acetone, there is a slight decrease in fracture toughness and slightly higher energy release rates. This change in performance could be due to the acetone slightly breaking down the epoxy compound. This method of adding acetone also reduces viscosity which could help with polymer infiltration. This combination could explain why the fracture toughness decreases but the energy release appears to be greater. It is quite possible that the bonding strength between the splats with epoxy was reduced lowering the fracture toughness, but with more epoxy present, the energy release values are slightly increased.

With additional acetone and toughener combined together in the template, there is a balance between that of the as sprayed template and the epoxy infiltrated template. The energy release rate has values that are placed right in between that of the as sprayed template and epoxy hybrid composite. Not only is there increased values over the as sprayed template but it also shows rising R-curve behavior which other epoxy hybrid composites have not demonstrated. It seems that the acetone reduced the viscosity allowing for higher infiltration but weakened the epoxy's strength. The toughener has a higher viscosity but increases the toughness of the hybrid composite. Since the viscosity of the toughener is high it limits how much of the epoxy mixture is able to be infiltrated in causing the crosslinking during heat treatment to be less effective. This however becomes quite beneficial since it allows for the hybrid composite to have rising R-curve behavior since the extrinsic mechanisms become effective.

7.3 Effect of template structure on fracture behavior

In order to further enhance the fracture performance of the template and hybrid composite, a reduction in the amount of spacing between layers was introduced by increasing material feed rate. The goal of this was to increase the density of template and thus increase fracture toughness but at the same time still allow epoxy infiltration. If the coating is made too dense, the epoxy would not be able to infiltrate in between the intersplat pores. Figure 7.6 shows the

microstructures at 300x (a & c) and 1000x (b & c) where (a) & (b) is for the standard spraying parameters and (c) & (d) is for the increase feed rate condition.

The microstructure of the increased feed rate has slight differences from that of the standard. The first difference is the change in amount and size of the layers. With the increased feed rate, there appears to more layers but thickness of each has decreased. In addition, the increased feed rate has appeared to have made the coating denser by decreasing the size of the intersplat pores. By comparing the 300x image of each template, the increased feed rate has a greater amount of globular pores.

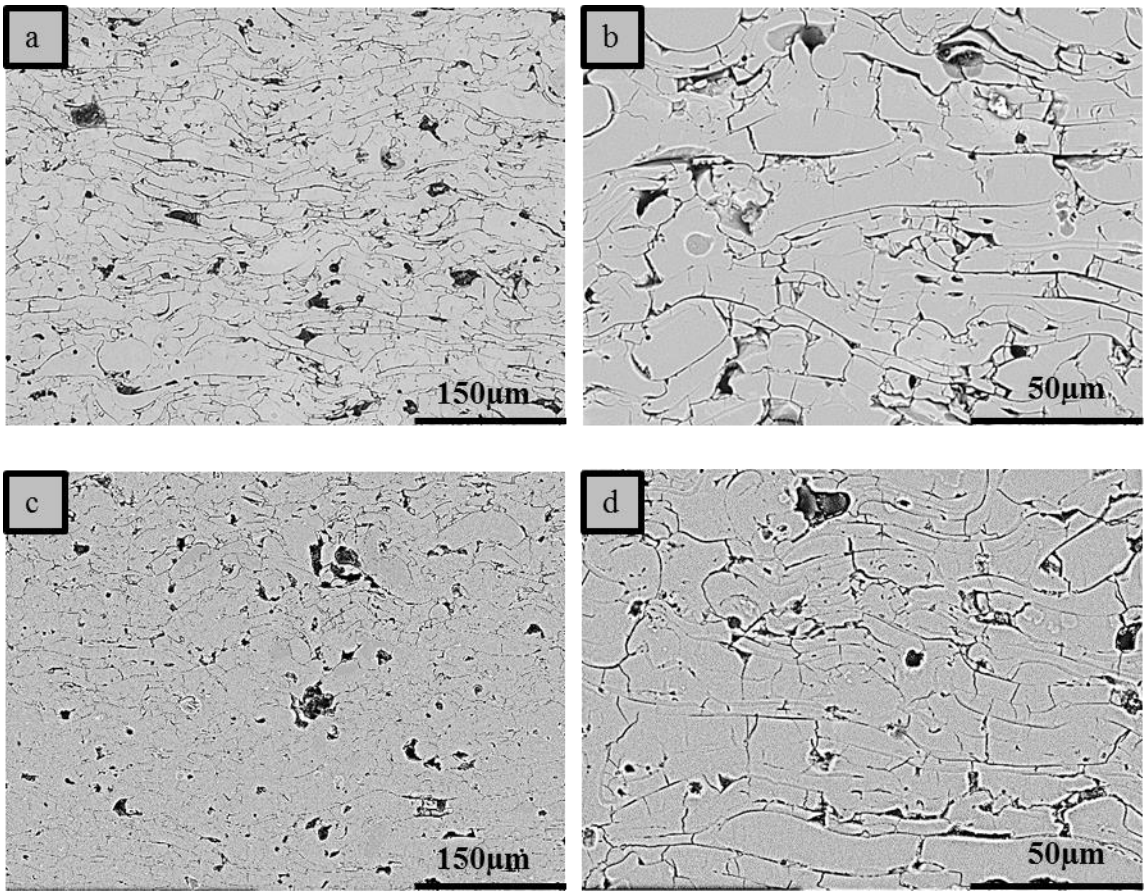

Figure 7.6: Microstructures at 300x and 1000x of both standard (a & b) and increased feed rate (c & d) condition templates

Figure 7.7 shows the fracture toughness (a) and corresponding load-displacement curves (b). The fracture toughness of the as sprayed increased feed rate template shows an increase going from 0.75 to 1.04 MPa-√m. When epoxy is infiltrated into the new template there is now a slight decrease in fracture toughness from 3.97 to 3.53 MPa-√m. Observing the load-displacement curves, there is no difference in fracture behavior. The as sprayed templates show similar "graceful" failure and the epoxy infiltrated hybrid composites undergo brittle failure.

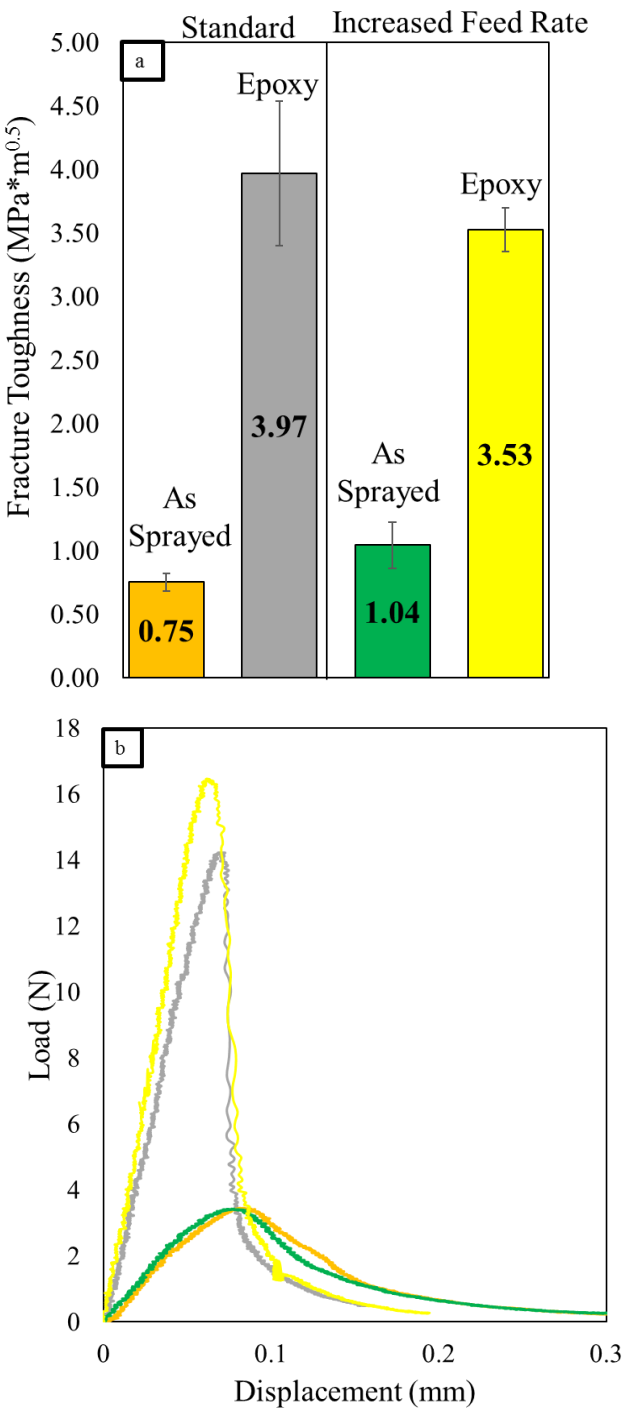

Figure 7.7: (a) Fracture toughness and (b) corresponding load displacement curves for both standard template and hybrid composite and high deposition rate (HDR) template and hybrid composite

Observing the energy release rates vs. notch extension curves shown in Figure 7.8, there is a slight increase, but nothing of significant change. While the initiation toughness is higher for the denser template, the rising R-curve behavior is less apparent. Both the epoxy infiltrated hybrid composites show similar energy release rate values and flat R-curve behavior.

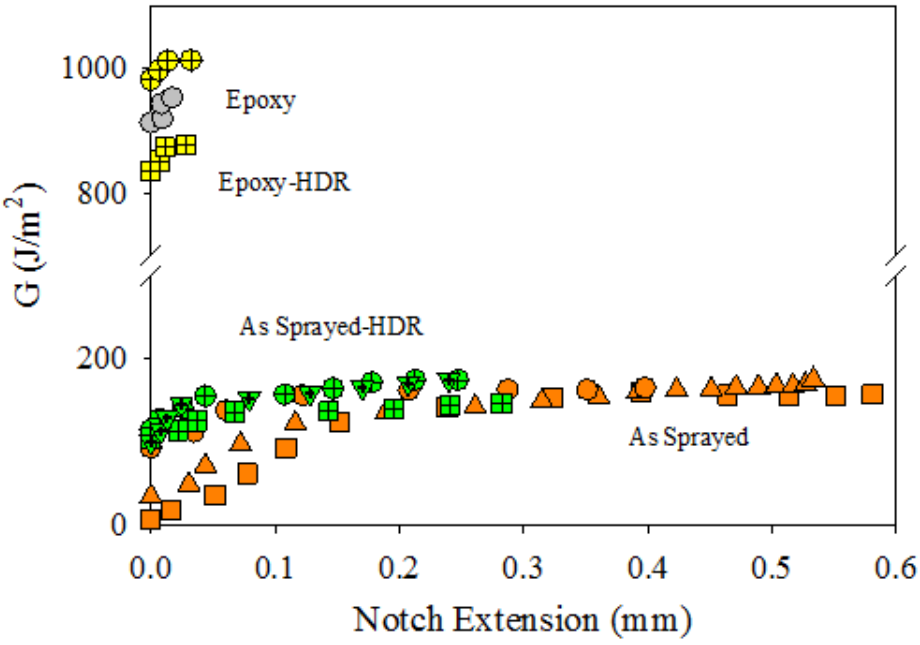

Figure 7.8: J-R Curves for both the standard and HDR template in the as sprayed and epoxy form.

Due to the denser structure of the new template, there is slight increase in toughness, but the behavior is still the same to that of the original template. The higher density allows the template to have a higher fracture toughness but still allow for it to display crack growth resistance due to the presence of numerous interfaces. This in turn allows the template to still be able to dissipate energy because of the platelets being able to slide during mechanical loading and crack propagation as well as previously mentioned mechanisms. However, the higher density does somewhat limit the amount of rising R-curve behavior as seen in Figure 7.8.

Since the high feed rate template is denser, it would be expected that less epoxy would be infiltrated lowering the fracture toughness much more. This unexpected result could be explained due to the fact that there even though the density is higher, there is still sufficient room for epoxy infiltration. While there is less room for infiltration, the higher fracture toughness of the denser template compensates for this.

7.4 Conlcusions

The material used to infiltrate a template and the way in which it is processed has the abilty to greatly influence the properties and beahvior of the hybrid composite. The as sprayed template showed low fracture toughness but experienced rising R-curve behavior due to the extrinsic toughening mechanisms of sliding and crack meandering. With the addition of epoxy, a substantail increase in fracture toughness was demonstrated but had flat R-curve beahvior since the extrinsic tougheing mechanisms are lost. A compromise of the two can be made by means of modifications and additives. This allows for a moderate increae in both fracture toughness and energy release rates while still having rising R-curve behavior with the use of the toughener and acetone. With the introduction of a denser template there is an increased fracture toughness and energy release rates of the as sprayed template, while still mainting a rising R-curve behavior. The denser strcuture does result in less notch extension in addition to slightly limiting the effects

of the epoxy. This occurs since the denser template incresaes the toughness but still allows for some epoxy infiltration. This denser templates compensates for the lower amount of epoxy infiltration which is why the toughness and energy release rates values only decrease somewhat. However, a problem with these solutions is the limitation of high tempeature application. The epoxy used with this template, can not go beyond 200ºC, thus another material must be used so three goals can be achieved. (1) The hybrid composite must have both a reasonable fracture toughness and energy releae rates. (2) The hybrid composite must have rising R-curve beahvior. (3) The hybrid composite must be able to withstand much higher operating temperatures for practical applications.

8 Fracture behavior of cermaic-metallic bio-inpsired hybrid composite

Since metals typically have both higher fracture toughness, its addition can enhance the overall fracture performance of a ceramic. Thermal spray being a layer-by-layer deposition process, such approach remains trivial with great feasibility. The fabrication of metal-ceramic composite also solves the temperature limitation issue associated with polymers. Since metals have a higher temperature tolerance they can be heat treated to further enhance the hybrid composites properties and behavior. However, it is important that the bonding between the ceramic and metallic components are not too strong so that the layers can still slide to dissipate the stored mechanical energy. To explore the effect of the metal toughening the hybrid composite, two hybrid composites (34% & 42% Al) were processed with different metal contents. Heat treatments were done with and without vacuum to understand how it affects the interactions between the metal and ceramic components.

8.1Effect of aluminum content in bio-inspired template

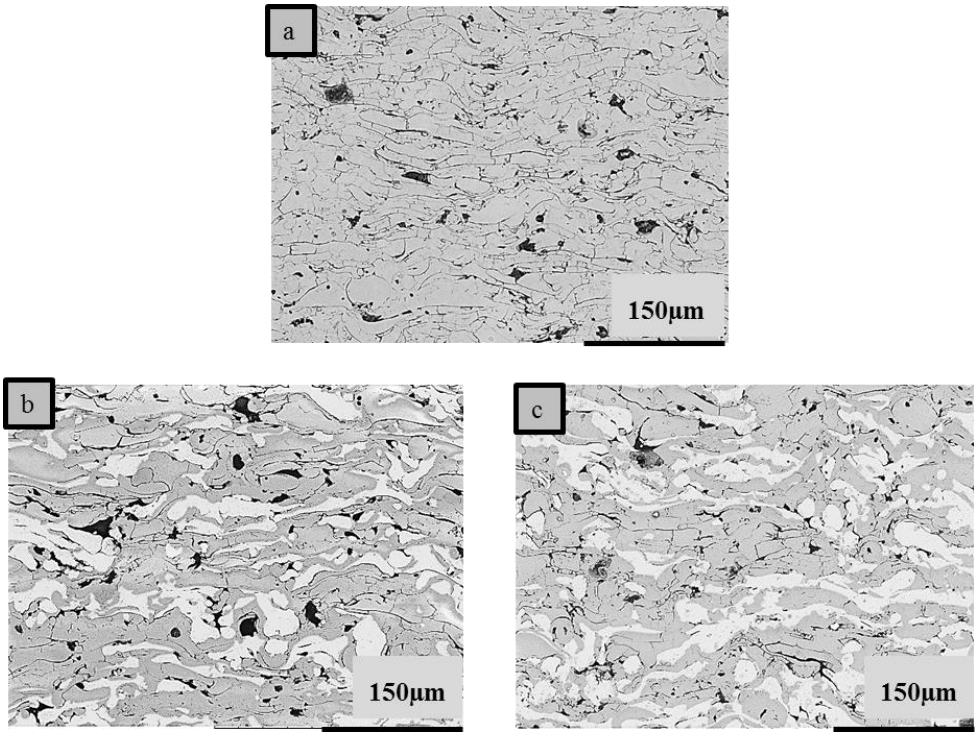

Figure 8.1: Microstructure for (a) standard template (b) hybrid composite with 34% Al and (c) hybrid composite with 42% at 300x

Three separate hybrid composites were tested which are the standard hybrid composite, and the two templates cosprayed with aluminum having 34% and 42% aluminum content by volume. Percent content was determined using optical images and imageJ software. Figure 8.1 shows the microstrucutres of each at 300x. (a) The standard ceramic template tested in chapter 7, (b) and (c) are the hybrid composites with 34% and 42% aluminum content. While, (b) and (c) do have similar features as the standard, such as globular and interlamellar pores and intersplat cracks and interfaces, the hybrid composites are not as ordered. The 42% aluminum content appears to have produced a denser structure with fewer globular pores.

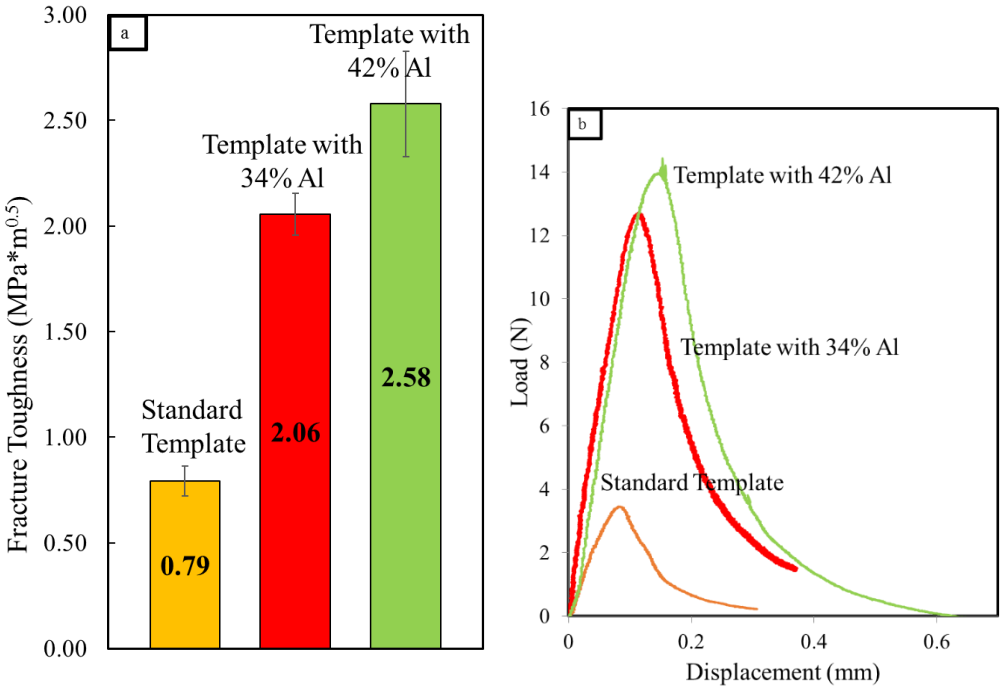

Figure 8.2: (a) Fracture toughness values of standard template and hybrid composites with 34% and 42% aluminum content. (b) Corresponding load-displacement curves.

While observing the J-R curves shown in Figure 8.3, the results correspond to the initial 3-point bend test for fracture toughness. The standard template, as shown previously, demonstrates a rising R-curve behavior, but has quite lower energy release values compared to the hybrid composites with aluminum. The 34% aluminum hybrid composite though shows values as much as six times as much as the previous template and while still maintaining a rising R-curve behavior. The 42% aluminum hybrid composite however, may show energy release values way above that of the 34% aluminum content, but has flat R-curve behavior.

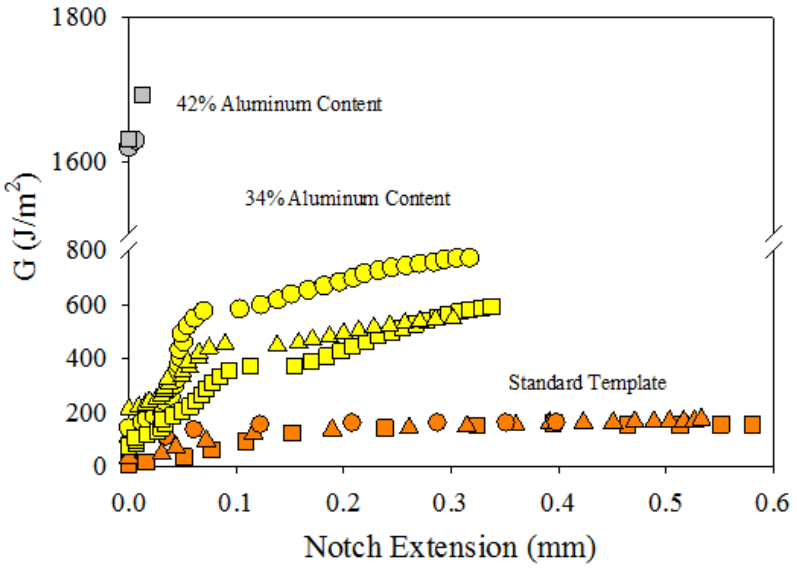

Figure 8.3: Energy release rate vs. notch extension curves for standard template and hybrid composites with 34% and 42% aluminum content.

Due to the inherent higher fracture toughness of metals, it is observed that there are higher values of fracture toughness with the 34% and 42% aluminum content added to the standard template. Naturally, with higher amounts of metal, the fracture toughness will be higher and as well as the energy release rates. However, what is interesting is that the fracture behavior of the 42% aluminum content hybrid composite. In theory, with higher amounts of metal, not only should the fracture toughness increase, but similar to the 34% aluminum content, the rising R-curve behavior should be present, which is not the case here. This can be possibly explained with the microstructure shown in Figure 8.1(c). Since the coating was denser and thus stiffer, it reduced the effects of the extrinsic toughening mechanisms present in the standard template, becoming unable to dissipate energy. This accounts for not only the lack of rinsing R-curve behavior but also as to why the energy release rates were significantly higher than that of the 34% aluminum content.

8.2 Effect of heat treatment on ceramic-metallic bio-inspired hybrid composites

With 34% aluminum

Since metals are able to operate at higher temperatures, a study was done by heat treating both metal hybrid composites at various temperatures to examine how the fracture toughness and R-curve behavior of each would be affected. By heating them past the melting point of the aluminum, it would hopefully be easier for the aluminum to flow in between the intersplat pores, similar to that of the epoxy. However, this can also cause the metal to flow outwards, leaving pockets where the metal was originally located. Temperatures much higher than melting point ($T_{melting}$ of Al6061 ~660^{o}C) were selected to understand the response of the aluminum by allowing it to flow more freely throughout the hybrid composite, as well as induce some mild sintering to the hybrid composite for additional toughness.

In order to further enhance the behavior of ceramic-metallic hybrid composites, heat treatments were done at 700ºC, 900ºC, 1000ºC, 1100ºC, and 1150ºC for two hours. It should be noted that heat treatment was also done at 800ºC but was left in the furnace accidently for three hours, so it was excluded. The study was first tested on the on the 34% aluminum content hybrid composite and based on these results, selected temperatures were done on the 42% aluminum hybrid composite. Figure 8.4 shows the microstructures of each hybrid composite at 100x. Comparing (a) to (b) and (c), not too much aluminum has flown out, but rather, has filled in some of the open porosity inside the hybrid composite. However, examining (d-f) a substantial amount of aluminum has flown out of the hybrid composite with some sintering occurring as well.

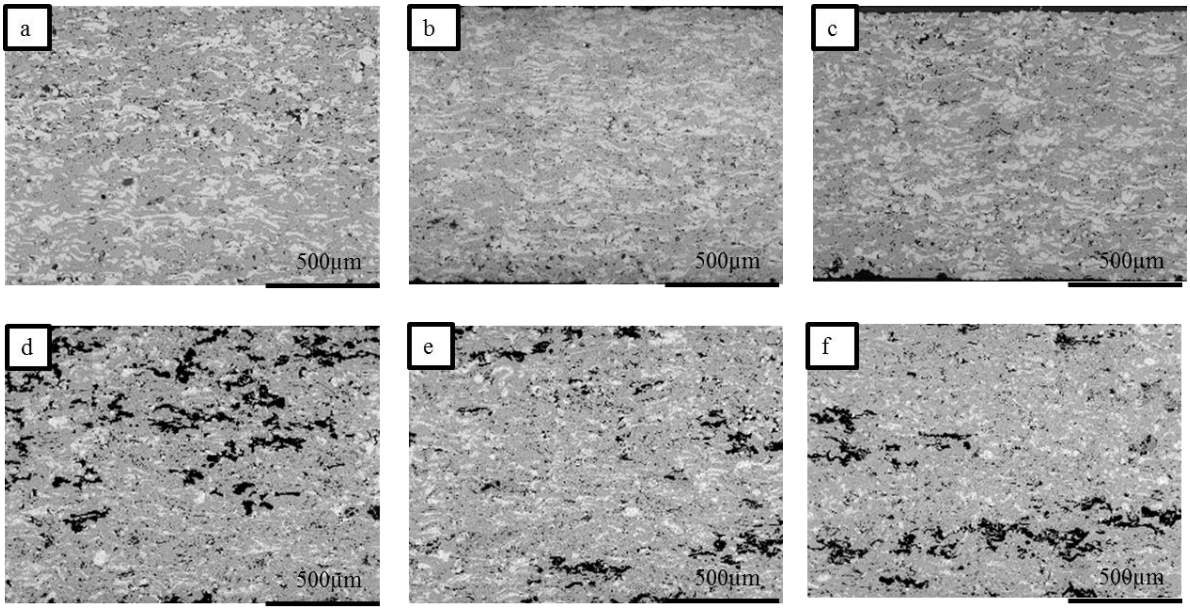

Figure 8.4: Microstructures of (a) as sprayed hybrid composite and hybrid composite heat treated at 700 (b), 900 (c), 1000 (d), 1100 (e), and 1150 (f) degrees Celsius at 100x

3-point bend testing was done on all heat treated hybrid composites and results from the test are shown in Figure 8.5(a). The results showed interesting results in which a linear trend with heat treatment did not occur. There is an optimal fracture toughness that occurred at 1000ºC, then dropped at 1100ºC, and increased again at 1150ºC. The values for fracture toughness starting with the as sprayed and then in order of increasing heat treatment temperature are 2.06, 2.79, 3.52, 4.02, 2.98, and 3.88 MPa-√m respectively. To confirm that there is a peak value at 1000ºC, each sample was tested using a micro-indenter to determine the hybrid composites' modulus as seen in Figure 8.5(b). The results from the micro-indenter showed the same trend as that of the fracture toughness values. The values are 95, 105, 188, 280, 154, and 218 GPa respectively.

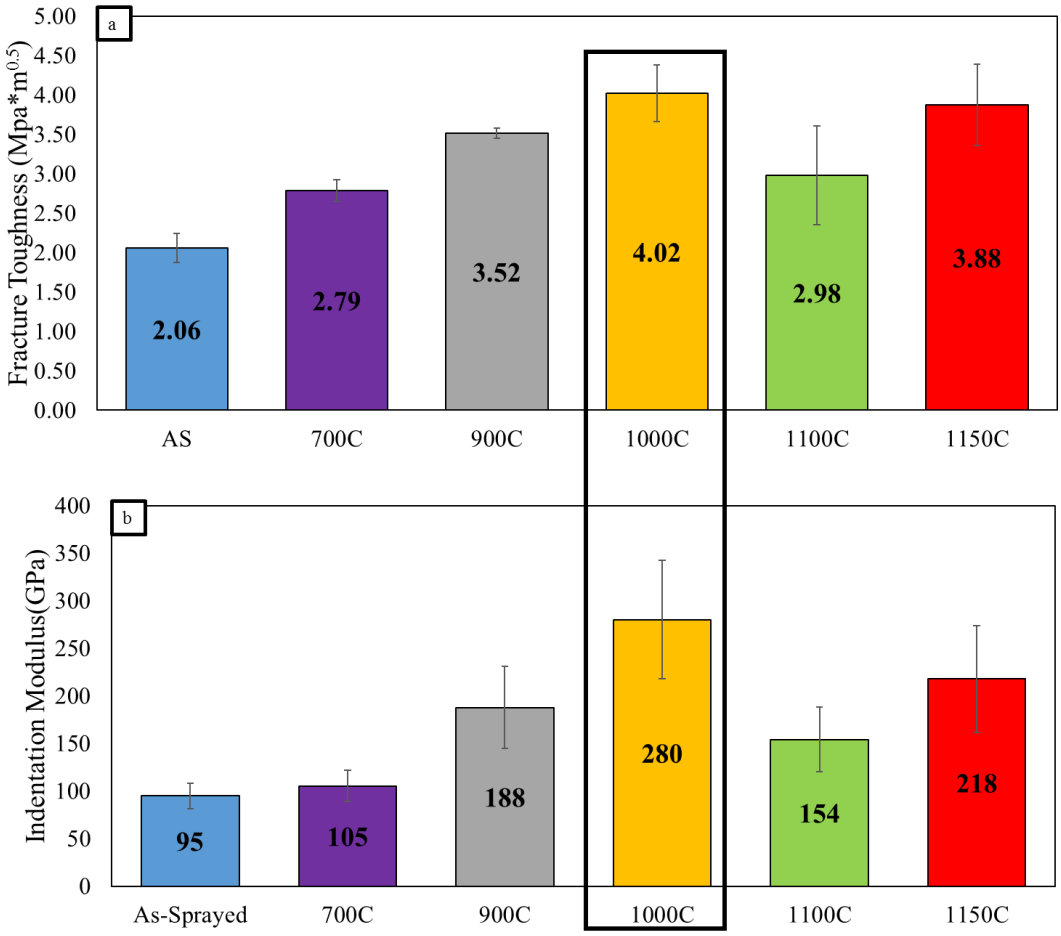

Figure 8.5:(a) Fracture toughness and (b) modulus values for the as sprayed hybrid composite and the various heat treatments of h it highlighting that there was an optimal value at 1000C.

Figure 8.6 shows the load-displacement curves from the fracture toughness testing for the as sprayed and heat treated hybrid composites. With increasing temperature, there is increasing stiffness of each hybrid composite. This means that with increasing heat treatment there is a transition from "graceful" failure to brittle failure. The transition appears to occur between 700ºC and 900ºC. Figure 8.7 shows the corresponding J-R curves for the as sprayed hybrid composite up to the heat treatments of 1000ºC. Curves for 1100 ºC and 1150 ºC were not shown due to not being able to obtain accurate data. Up to 900 ºC, there is rising R-curve behavior. At 1000 ºC, there is barely any rising R-curve behavior.

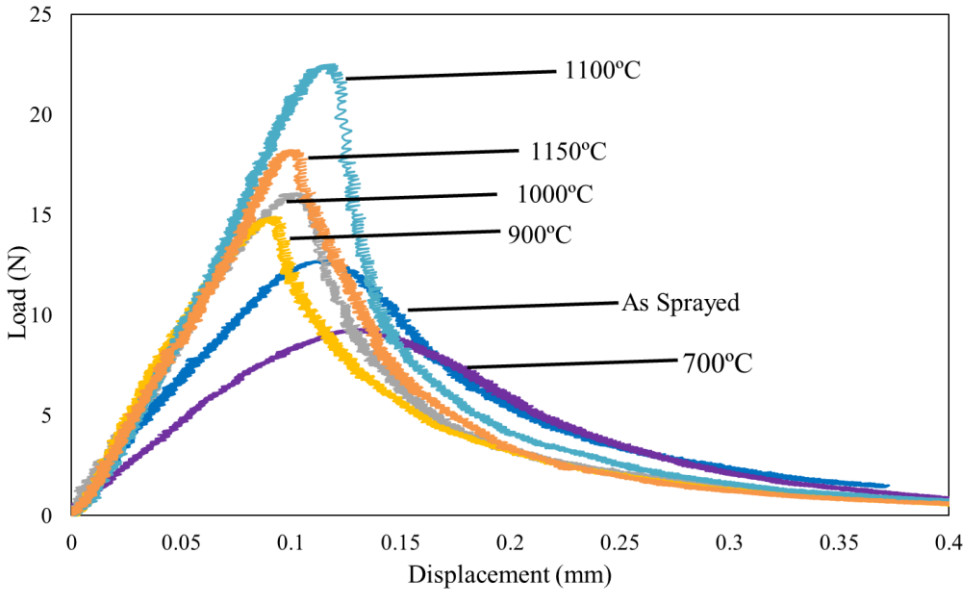

Figure 8.6: Load-Displacement curves from fracture toughness testing of as sprayed and heat treated hybrid composites

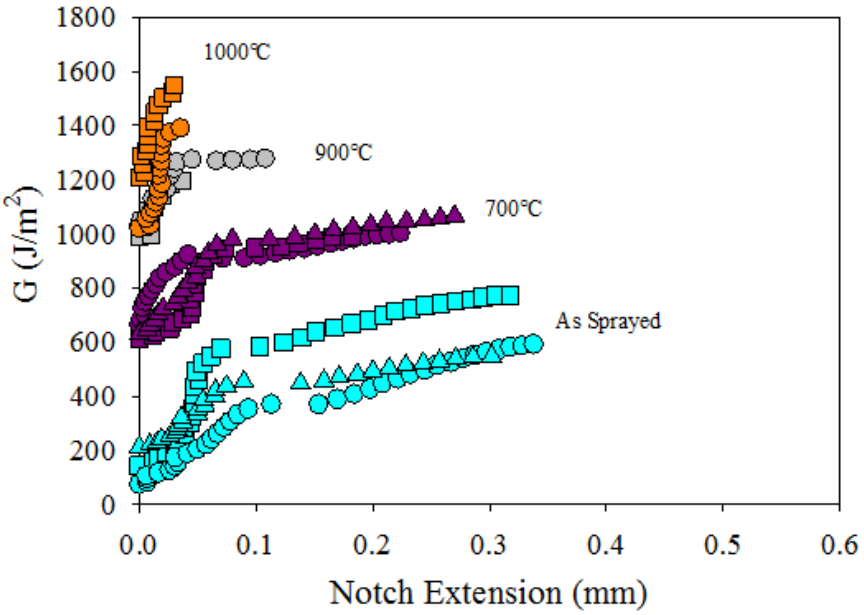

Figure 8.7: J-R curves of as sprayed hybrid composite and heat treatments up to 1000C.

There is an optimal value for fracture toughness and modulus when the hybrid composite is heat treated to 1000 ºC. This occurs possibly due to a combination of the aluminum flowing into pores while only a minimal amount flows out of the hybrid composite in addition to some mild sintering. It is also possible that during the heat treatment the aluminum is oxidizing into alumina, further strengthening the hybrid composite. This can be seen in Figures 8.6 and 8.7 that the stiffness of the material has increased but still have some amount of rising R-curve behavior. This decrease from 1000ºC to 1100ºC happens due to the amount of aluminum that has been lost

with mild sintering. It is observed that there is an increase at 1150 ºC because more sintering is occurring which makes up for the loss of aluminum. Between 1100 ºC and 1150 ºC, there is not much change due to the slight change in temperature, but additionally, there is not linear trend as shown with the peak fracture toughness and modulus at 1000 ºC.

These same explanations can be used to understand the R-curve behavior as well. At 700 ºC, a marginal increase in energy release rates while the specimen still maintained its rising R-curve behavior. This happens due to the aluminum mostly flowing into the pores of the hybrid composite and slightly oxidizing the aluminum. At 900 ºC, it is observed that there is increasing energy release rates but much less rising R-curve behavior. At this point, the amount of aluminum lost is more substantial and more aluminum could be oxidized. By the time heat treatment occurred at 1000 ºC a substantial amount of aluminum is lost and with more sintering occurring there are have higher energy release rates but minimal rising R-curve behavior. In other words, with increasing temperature, there is increased bonding between the layers in addition to sintering, which results in the reduction of extrinsic toughening.

With 42% aluminum

Applying what was observed from the previous study, only two temperatures were used to study the effects on toughness of this hybrid composite (43% Al). Figure 8.8 shows the microstructures for (a) the as sprayed hybrid composite, (b) the hybrid composite heat treated at 700 ºC and (c) the hybrid composite heat treated at 1000 ºC. Observing (a) and (b) there is no significant change in structure but when you compare them to (c) the concentration of aluminum has dispersed and even flown out of the hybrid composite. Taking a closer observation at (c) it is noticeable that coating appears to have become denser due to some sintering occurring during the treatment.

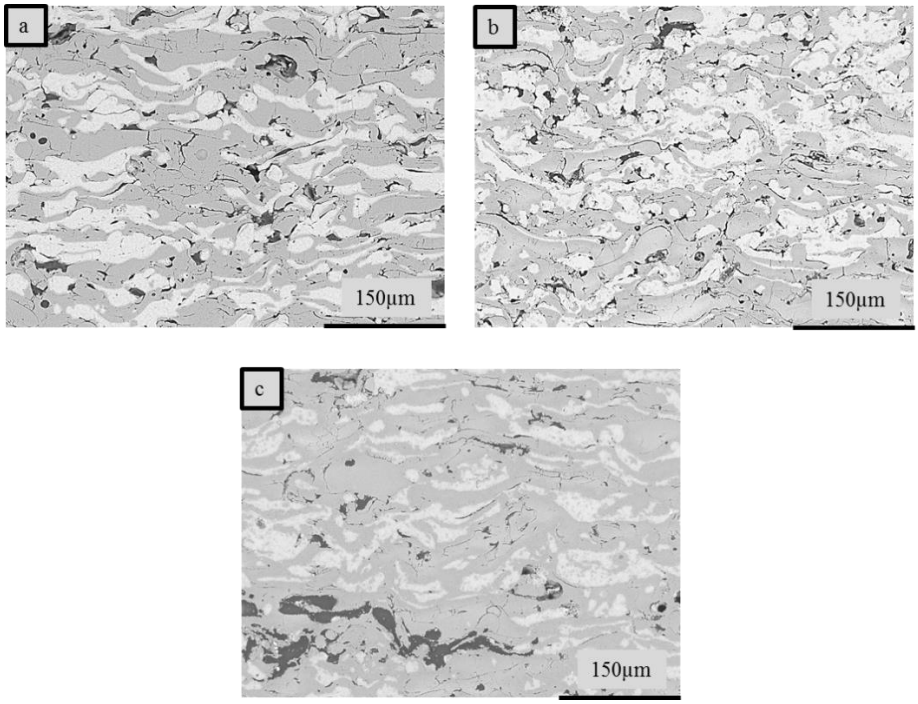

Figure 8.8: Microstructures of (a) as sprayed hybrid composite, (b) hybrid composite heat treated at 700˚C and (c) hybrid composite heat treated at 1000 ˚C at 300x

Figure 8.9 shows the fracture toughness values for each hybrid composite tested (a) and their corresponding load-displacement curves (b). When comparing both the as sprayed and 700 ˚C heat treated hybrid composite, there is no significant change in fracture toughness and behavior. The as sprayed has a fracture toughness of 2.58 MPa-√m while the hybrid composite heat treated at 700 ˚C has a value of 2.82 MPa-√m. When observing the load-displacement curves they both demonstrate the same type of "graceful" failure. When the hybrid composite is heat treated at 1000 ˚C, there is a substantial increase in fracture toughness and a change in fracture behavior. The fracture toughness rises to 4.09 MPa-√m and a transition from a "graceful" behavior to that of a more brittle failure.

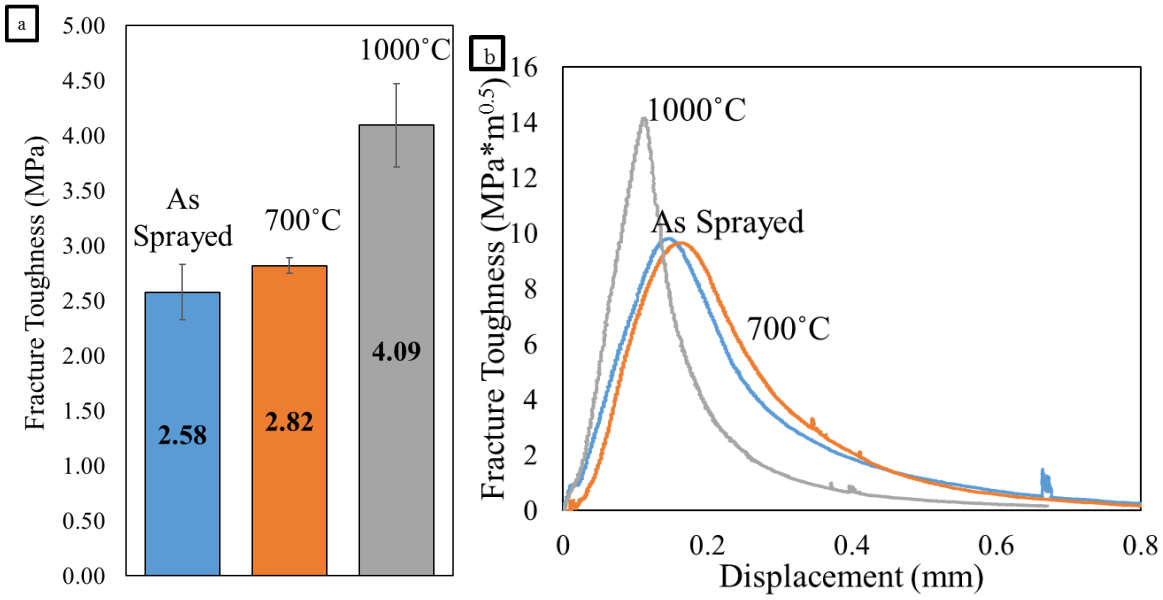

Figure 8.9:(a) Fracture toughness values of the as sprayed hybrid composite and heat treatments at 700˚C and 1000 ˚C. (b) corresponding load-displacement curves

Observing Figure 8.10, all of the hybrid composites have flat R-curve behavior. The as-sprayed hybrid composite and heat treated hybrid composite at 700˚C show similar crack growth and energy release rates. When the hybrid composite undergoes heat treatment at 1000 ˚C, there is an increase in release rates but even less crack growth. Since the hybrid composite before heat treatment, had flat R-curve, it was expected that the heat treatments would demonstrate this behavior as well.

Due to the as sprayed hybrid composites already having dense structures, there is limited mobility for layers to slide and crack meandering to occur, resulting in no extrinsic toughening. While this may result in higher fracture toughness values, it gives the hybrid composite a flat R-curve behavior. Upon heat treatment there is an increase in fracture toughness due some of the metal flowing into the pores and at higher temperatures, sintering the hybrid composite to increase density, but also losing the majority of the metal content. These high temperatures allow for a great increase in fracture toughness and energy release rates, but further make the hybrid composite brittle upon failure.

Another possible reason for the aluminum outflowing besides it melting, is that alumina does not bond well with aluminum. While the poor bonding between alumina and aluminum may be useful at the as sprayed condition where the layers able to move to some extent, it is negative for the heat treatments since the aluminum would want to flow out. There is also the issue of any

oxidation of aluminum, which may increase the strength, but can also make the hybrid composite brittle, resulting in flat R-curve behavior. In an attempt to help counteract this, the next section of this chapter will do a similar heat treatment study, but instead in vacuum.

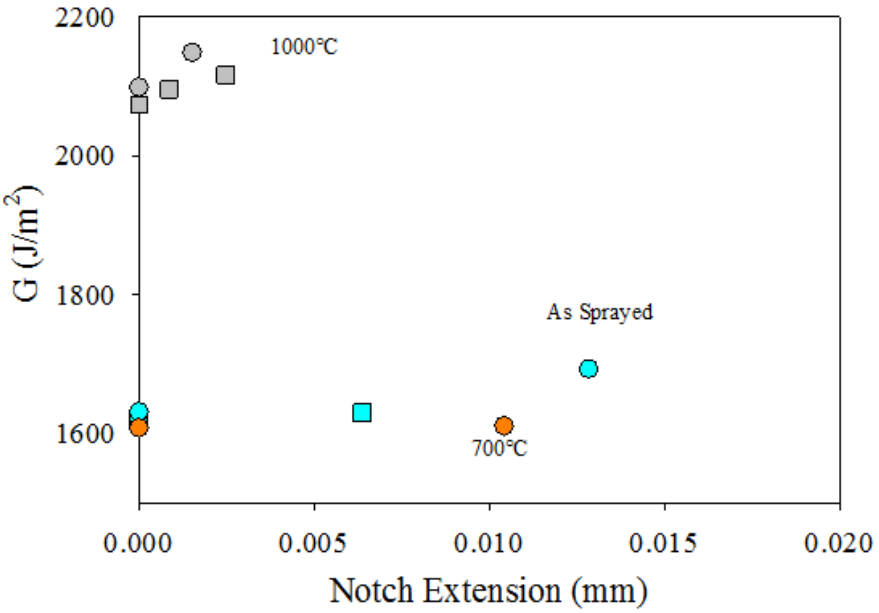

Figure 8.10: Energy release rate vs. notch extension curves for as sprayed and heat treatments.

8.3Effect of in vacuum heat treatment on ceramic-metallic bio-inspired hybrid composite

With 34% aluminum

Vacuum heat treatment of the hybrid composite was done at both 700˚C and 1000 ˚C for two hours. As mentioned earlier, the selection of these temperatures were based on the results from the earlier section. Microstructures of each hybrid composite can be seen in Figure 8.11 with (a) as sprayed hybrid composite and (b & c) hybrid composite vacuum heat treated at the previously mentioned temperatures. Comparing (a) and (b), there is not much of a difference except there a slight loss in aluminum. However, in (c), a more noticeable amount of aluminum is missing but not as much in air heat treatment specimen at the same temperature (Figure 8.4).

Figure 8.12 shows the fracture toughness (a) and the corresponding load-displacement curves (b). At 700 ˚C there is a slight increase in fracture toughness from 2.06 to 2.53 MPa-√m. There is also similar behavior when failure occurs in which “graceful” failure is being observed. When heat treated to 1000 ˚C, a steep increase in fracture toughness up to 4.64 MPa-√m is observed. With the increase of fracture toughness though, a transition from “graceful” failure to brittle failure was noticed. Compared to the in air heat treatments, similar load-displacement curves and fracture toughness values at 700 ˚C, but at 1000 ˚C there is a higher fracture toughness with the vacuum.

Figure 8.13, shows the energy release rate vs. notch extension curves. For both 700 ˚C and 1000 ˚C vacuum heat treatments there are increased energy release rates compared to the in air treatments. However, even though there is an increase in energy release rates, there is no slow

crack growth. While it is beneficial to have higher energy release rate, the hybrid composite exhibits flat R-curve behavior.

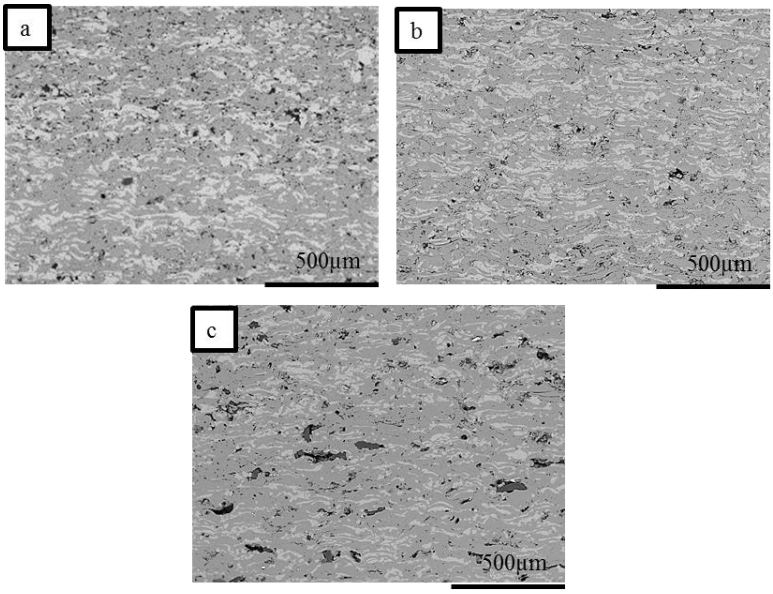

Figure 8.11:Microstructures (a) as sprayed hybrid composite, (b & c) vacuum heat treated at 700˚C and 1000 ˚C at 100x

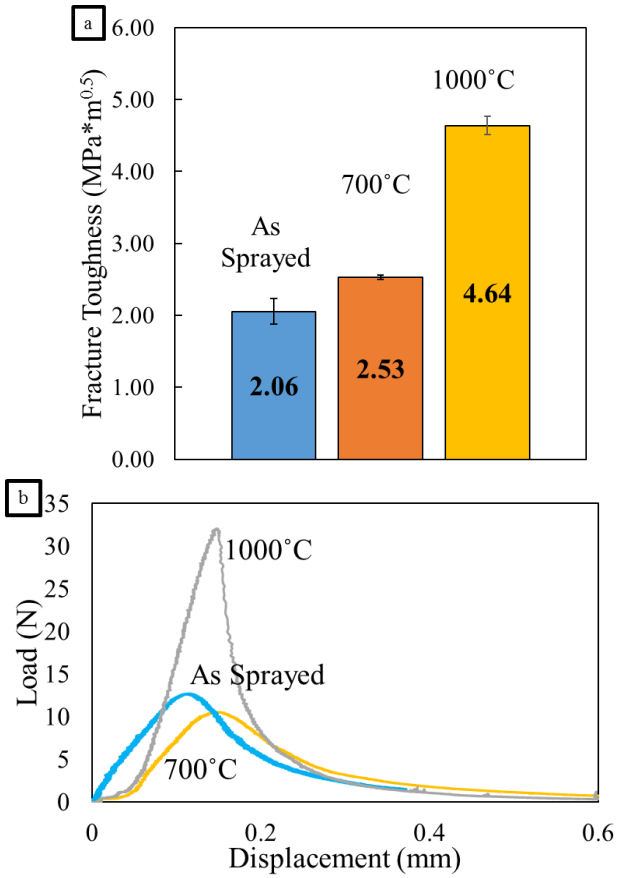

Figure 8.12: (a) fracture toughness values of each hybrid composite tested with (b) their corresponding load-displacement curves.

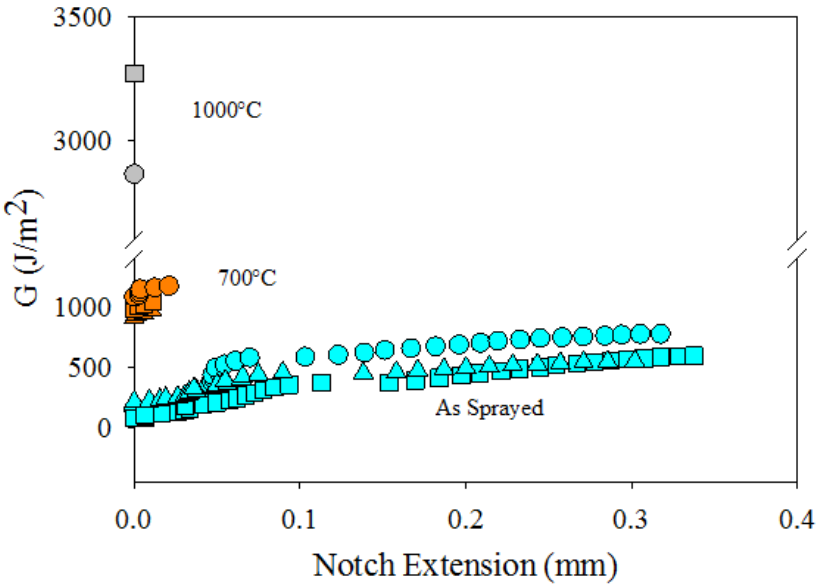

Figure 8.13: J-R curves for the as sprayed hybrid composite and the ones vacuum heat treated at 700˚C and 1000 ˚C

With vacuum heat treatment, there are changes to fracture toughness and behavior. Fracture toughness values have slightly increased due to less aluminum loss and better bonding between the ceramic and metallic components. With vacuum heat treatment an increase in energy release rates is seen, but loss of rising R-curve behavior. Heat treating in vacuum limits the metal from out flowing and enables movement within the hybrid composite. This effect allows for stronger bonding between the layers, limiting any toughening mechanisms that could be occurring, meaning that fracture toughness is increasing, but at the cost of having no rising R-curve.

With 42% aluminum

Hybrid composite was vacuum heat treated at 700 ˚C and 1000 ˚C for two hours just as the 34% aluminum content hybrid composite. Figure 8.14 shows the microstructures of the hybrid composites at 300x. At 700 ˚C (b) there is open porosity due to the aluminum flowing out. At 1000 ˚C (c) more aluminum has flown out but at the same time the hybrid composite has gone under sintering, making it denser and stiffer.

Examining the fracture toughness values in Figure 8.15(a) there are differences from the standard (42% aluminum) with heat treatment performed without vacuum. At 700ºC there is a slight increase from 2.58 to 2.95 MPa-√m. With vacuum heat treated at 1000 ºC however, there is a significant increase in fracture toughness. The hybrid composite rises up to 5.71 MPa-√m. Observing the load displacement curves (b) it is observed that the as sprayed and 700 ºC heat treated hybrid composite behave similarly having slight “graceful” failure. With the 1000 ºC treated hybrid composite, there is a sharp brittle failure.

Figure 8.16 shows the J-R curves for the as sprayed and heat treated hybrid composites. The as sprayed hybrid composite exhibits flat R-curve behavior. Heat treatment at 700 ºC, results in increased energy release rate and once again flat R-curve behavior is present. Heat treatment at 1000 ºC causes is a substantial increase in energy release but similar to the other two, flat R-curve behavior is present.

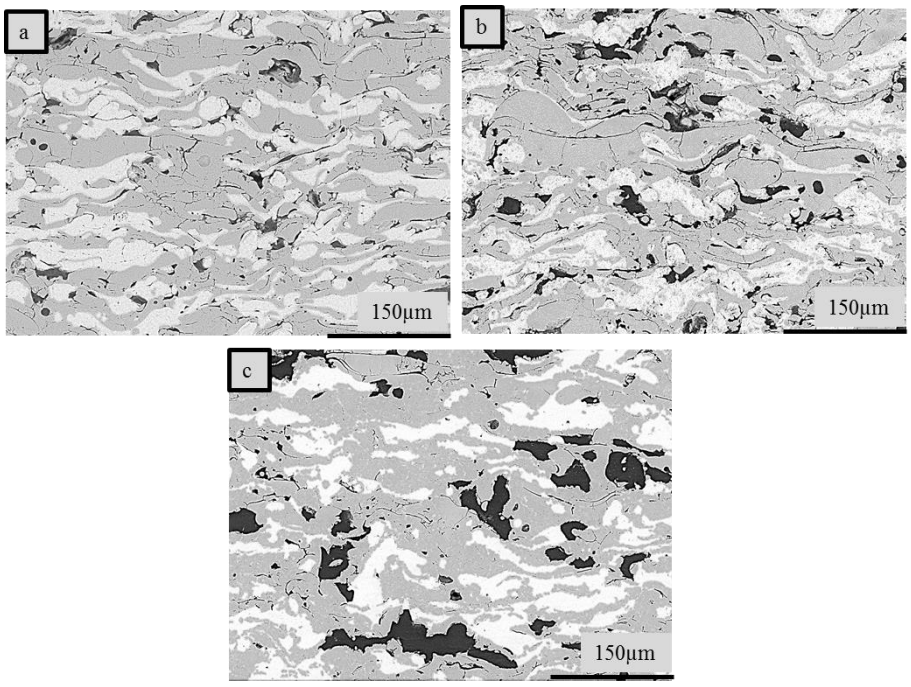

Figure 8.14: Microstructure images of as sprayed hybrid composite (a) and vacuum heat treated hybrid composites at 700˚C (b) and 1000 ˚C at 300x (c)

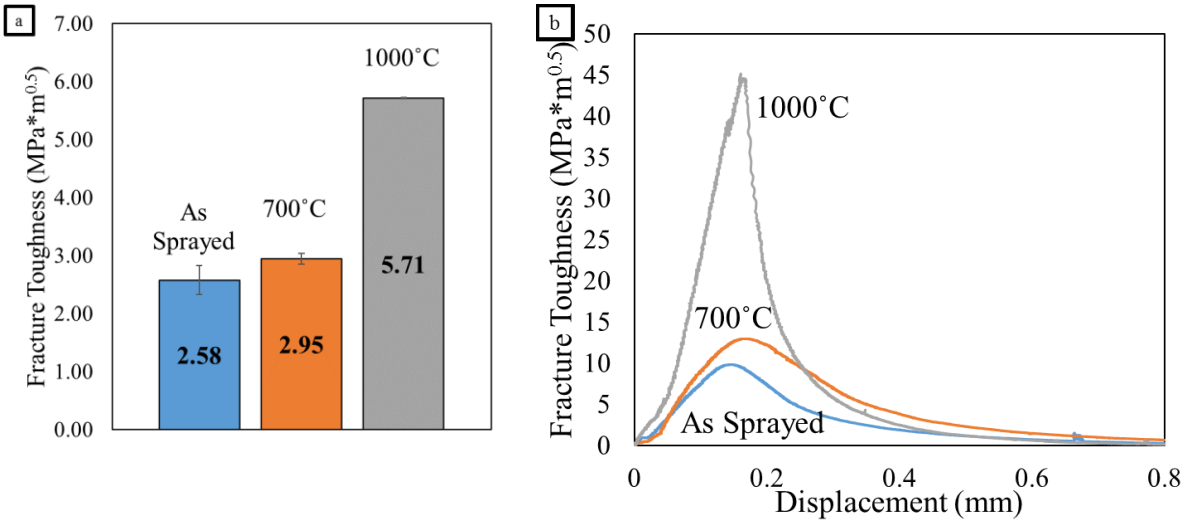

Figure 8.15: (a) Fracture toughness values of as sprayed and vacuum heat treated hybrid composites and (b) corresponding load-displacement curves.

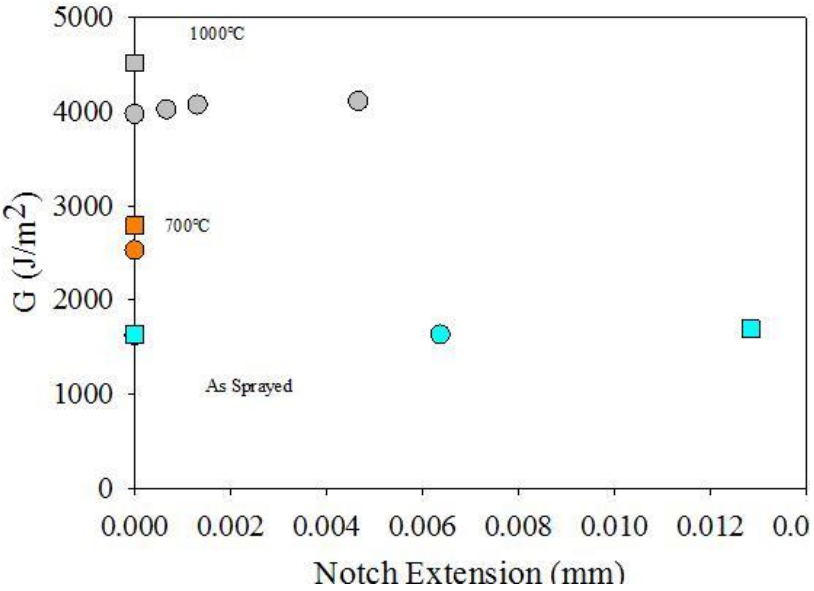

Figure 8.16: Energy release rates vs. notch extension for as sprayed and vacuum heat treated hybrid composites.

The use of vacuum heat treatments seems to have some benefit to the fracture toughness and energy release rate of the hybrid composite. The vacuum allows for better flow of the aluminum instead of all it flowing out of the hybrid composite due to the external pressure caused by the vacuum. Without the effect of the air, the aluminum also does not oxidize as much, toughening the hybrid composite. Since the bonding between the layers has been strengthened, the hybrid composite becomes increasing stiffer, resulting in higher energy release rates with flat R-curve behavior however.

8.4 Conclusion

With the addition of aluminum, there is both an increase in fracture toughness and energy release rates. However, rising R-curve behavior was only exhibited with the 34% aluminum content since the hybrid composite was not as stiff allowing for the extrinsic toughening mechanisms, such as interface sliding, to reduce the driving crack force. With the 42% aluminum content there is higher values of fracture toughness and energy release rates but at the cost of flat R-curve behavior. This occurred due to the better bonding between the metal and ceramic components, inhibiting the extrinsic toughening mechanisms.

With heat treatment without vacuum it was determined that there is an optimal heat treatment temperature to maximize fracture toughness and energy release rates. When heat treating at 1000 ºC however, there is rising R-curve behavior is greatly reduced. With lower temperatures for the 34% aluminum content, there is a balance of increased fracture toughness and rising R-curve behavior. When it comes to the 42% aluminum content there is flat R-curve behavior even without heat treatment so with the addition of heat treatment, there is further stiffening of the hybrid composite.

When heat treatment is done at vacuum, it further enhances fracture toughness, but at the cost of flat R-curve behavior. This occurs due to the better bonding between the metal and ceramic portions making the hybrid composite stiffer causing the extrinsic mechanism to be efficient. The 42% aluminum content appears to benefit more from vacuum especially at 1000 ºC when the

fracture toughness reaches 5.71 MPa-√m which is the highest recorded toughness in this study. Naturally, it also has the highest energy release rate values.

9. Summary and conclusions

Previous work done has shown that using thermal spray, a brick-&-mortar structure resembling nacre can be synthesized. This hybrid composite has similar mechanical behavior and properties to nacre as well. Based on the above statements and the mechanisms mentioned previously during crack propagation, the material could have rising R-curve behavior meaning upon crack propagation significant amount of stored energy is dissipated which in turn slows down the crack extension. In order to evaluate the behavior, a 3-point bend method following ASTM standards and the secant compliance method were used to calculate the energy release rates and notch extension of a pre-notch sample, respectively.

After validating the method, both the as sprayed and epoxy infiltrated templates were tested to plot their J-R curves. Results showed that the as sprayed template exhibited a rising R-curve behavior while the infiltrated template does not. This extrinsic toughening mechanism of the layers being able to slide against each other and the crack meandering in the as sprayed template are the result of the weak bonding between the layers, causing the rising R-curve behavior. In addition, as a result of this toughening, crack bridging, branching, and blunting may occasionally be active,

The epoxy infiltrated template, while having increased strength and toughness, lacks this rising R-curve behavior because of the additional bonding strength from the epoxy. This results in the hybrid composite to have a high initiation toughness, but a lack of extrinsic toughening mechanisms. This also suggests that in order to increase the toughness of the material, there is a need to introduce strong binder for layer interfaces, but not so strong that the main component can still slide as well as experience crack meandering to dissipate energy to have rising R-curve behavior.

In order to allow the infiltration to be more effective, the epoxy was modified by adding acetone which would lower its viscosity of it. This was done in order to allow more epoxy to infiltrate into the template and as well as potentially weaken the bonding between the layers, allowing for extrinsic toughening mechanisms to remain effective. The results showed that there was no significant change in the hybrid composite's mechanical properties or behavior, possibly because after acetone evaporation, the epoxy became stronger again. The use of epoxy with toughener and acetone was then determined to be used since it has a lower viscosity but higher toughness compared to the untreated epoxy. Acetone was used to reduce the overall viscosity to allow more of the mixture to infiltrate. The result was an increase in fracture toughness of hybrid composite while having some rising R-curve behavior. The values were higher than the as sprayed but not as much as the standard epoxy. This occurs due to the bonding of the epoxy mixture to the ceramic matrix to be weaker in presence of the toughener than that of the standard epoxy.

By alternating the epoxy there was a balance of fracture toughness and rising R-curve behavior. Further, it was also observed that by making the template denser, there was a slight increase in fracture toughness and rising R-curve y-axis values. Even though the density

increased, extrinsic toughening mechanisms were able to occur. When epoxy is infiltrated, the fracture toughness decreased but there was still flat R-curve behavior, similar to that of the standard hybrid composite with epoxy. The denser template allows for less epoxy infiltration but is compensated by the denser structure.

The approach to designing a ceramic hybrid composite with rising R-curve behavior is to produce an interface in between the layers that strengthens the material but not to the point where the energy dissipation of interlayer sliding and crack meandering are not effective. Using epoxy can be effective but there is limitation of both temperature usage and infiltration. To overcome this, co-spraying with aluminum was chosen to increase fracture toughness and maintain rising R-curve behavior and allow for the use at higher operating temperatures.

Two separate hybrid composites were done with varying amounts of aluminum content (34% & 42% vol.) to examine how it would affect the toughness and R-curve behavior. With 34% aluminum content, there is increased fracture toughness while still having rising R-curve behavior. Metals typically have higher toughness since they are able to plastically deform to release energy. It is possible that the bonding between the alumina and aluminum is not too strong that the effects of interlayer sliding and crack meandering still remain possible. The increased fracture toughness and energy release rates most likely stems from the higher fracture toughness of the aluminum and the right amount of increased bonding strength between the aluminum and alumina.

When 42% aluminum is present there is increased toughness but flat R-curve behavior. Observing the microstructure, the hybrid composite appears to be denser than that of the hybrid composite with 34% aluminum. This stiffer hybrid composite reduces the ability of the extrinsic toughening mechanisms. What is interesting is that metals have higher fracture toughness so adding more should make it more effective but the increased the bonding strength between the layers was too strong, resulting in flat R-curve behavior.

Since the purpose of aluminum was to also increase the temperature capabilities of the hybrid composites, the effect of heat treatment on these hybrid composites were examined. The two hybrid composites were heat treated at various temperatures selectively from 700C to 1150C. In terms of fracture toughness, there was an optimum value when heat treated at 1000˚C which may be due to the aluminum being able to flow into the interlamellar pores of the hybrid composite along with some mild sintering of the overall structure. At this temperature however, there is only slight rising R-curve behavior due to the increased bonding between the layers. In fact, it is observed that with additional increase in heat treatment temperature, there is a reduction in rising R-curve behavior. After testing the 42% aluminum content hybrid composite, the fracture toughness increases but there is no change in R-curve behavior. Since at the as sprayed condition (42% aluminum compared to 34% or the standard ceramic template) already had strong bonding in between the layers, heat treatment further increased the bonding and toughness, causing no transition from flat to rising R-curve behavior.

Vacuum heat treatment was done at similar temperatures to understand how the absence of oxidation would affect the fracture toughness and R-curve behavior of the hybrid composites. For both hybrid composites, the fracture toughness increased much more than the treatment without vacuum, but none produced any rising R-curve behavior. Since minimal oxidation of the aluminum as well as the external pressure from vacuum helped the metal to flow better throughout the coating, which resulted in better bonding between the layers, causing the extrinsic toughening mechanisms to be ineffective.

In summary, using thermal spray, it is possible to produce ceramic and ceramic composites to design materials with rising R-curve behavior. With the processes used in this thesis, the scaled up synthesis and production of these nature-inspired hybrid composite is highly feasible. Although the coatings produced do exhibit rising R-curve behavior, their fracture toughness values remain quite low compared to that of bulk or other produced composites due to presence of several weak interfaces, which add to the design criterion of these hybrid composites. These interfaces, on one hand reduce the materials strength against fracture, they do offer opportunities to introduce the tougher media at those interfaces and hence tunable fracture toughness of the hybrid composites.

10 Future work

Results shown previously have indicated that, by synthesizing a composite via thermal spray, simultaneous increment in terms both fracture toughness and strength can be achieved. This study further added strategies, such as loose interface and addition of metallic phases, to develop hybrid composites which also have crack growth resistance. This was quantified in terms of their R-curve behavior. This section will discuss how to enhance the current method to produce a coating with both increased fracture toughness and more pronounced rising R-curve behavior and as well as other materials instead of aluminum to enhance it.

10.1 Modification to ceramic composite design

The results showed that the composites designed were able to experience rising R-curve behavior when processed properly with thermal spray. While rising R-curve behavior was present, the hybrid composites did not have high fracture toughness values as shown in the Figure 1.9. Using thermal spray, it is not expected to get bulk values but it is still possible to get values in their range. In order to enhance the current composite design, three new approaches should be studied further.

1. Adjust particle size of aluminum.
2. Use of different metals.
3. Co-spray with another ceramic instead of a metal.

As stated in the introduction section for toughening mechanisms for ceramic composites, ductile phase toughening can be used to enhance the toughness of the main ceramic component. With the addition of metal, the composite exhibited increased initiation toughness while maintaining slow crack growth mechanisms. This is seen in the alumina-aluminum composite when there is 34% aluminum content present. With thermal spray, the hybrid composites can be fabricated using different particle sizes and the previously mentioned toughening mechanism can work better with smaller particle sizes. Therefore, a study can be conducted with smaller aluminum particles to potentially increase the fracture toughness and rising R-curve behavior further. With the use of smaller particle sizes, the concentration of aluminum components in the main ceramic matrix, should not interfere with the ordered structure as much, toughening the hybrid composite.

Using metals with higher fracture toughness can be another approach to increase fracture toughness but still have rising R-curve behavior since it has already shown that it works with metal. Work has already been started and will be pursued in future work, by co-spraying with nickel (Diamalloy 1007, d50=65µm, Oerlikon Metco, Westbury, NY) copper (Ni-114, d50=80µm, Praxair, Indianapolis, IN) and aluminum with 5% magnesium silicide (Part98%+ Magnesium Silicide, d50=12 µm, American Elements, Los Angeles, CA) as shown in Figure 10.1 which shows microstructures of each at 100x. Powder size and feed rate was constant for

each. Comparing the hybrid composite with aluminum (a) and aluminum with 5% Mg_2Si (b) there is no difference in structure and appeared similar to the structure produced in chapter 8 with 34% aluminum. However, examining the copper-alumina composite (c) it appears that there is a higher amount of metal content and the concentration of metal appears larger. Nickel (d) on the other hand produced smaller concentrations of metal content and size as well as more porosity. Note that these microstructures are from a preliminary trials and may not be optimized, however they do serve as a proof-of-concept.

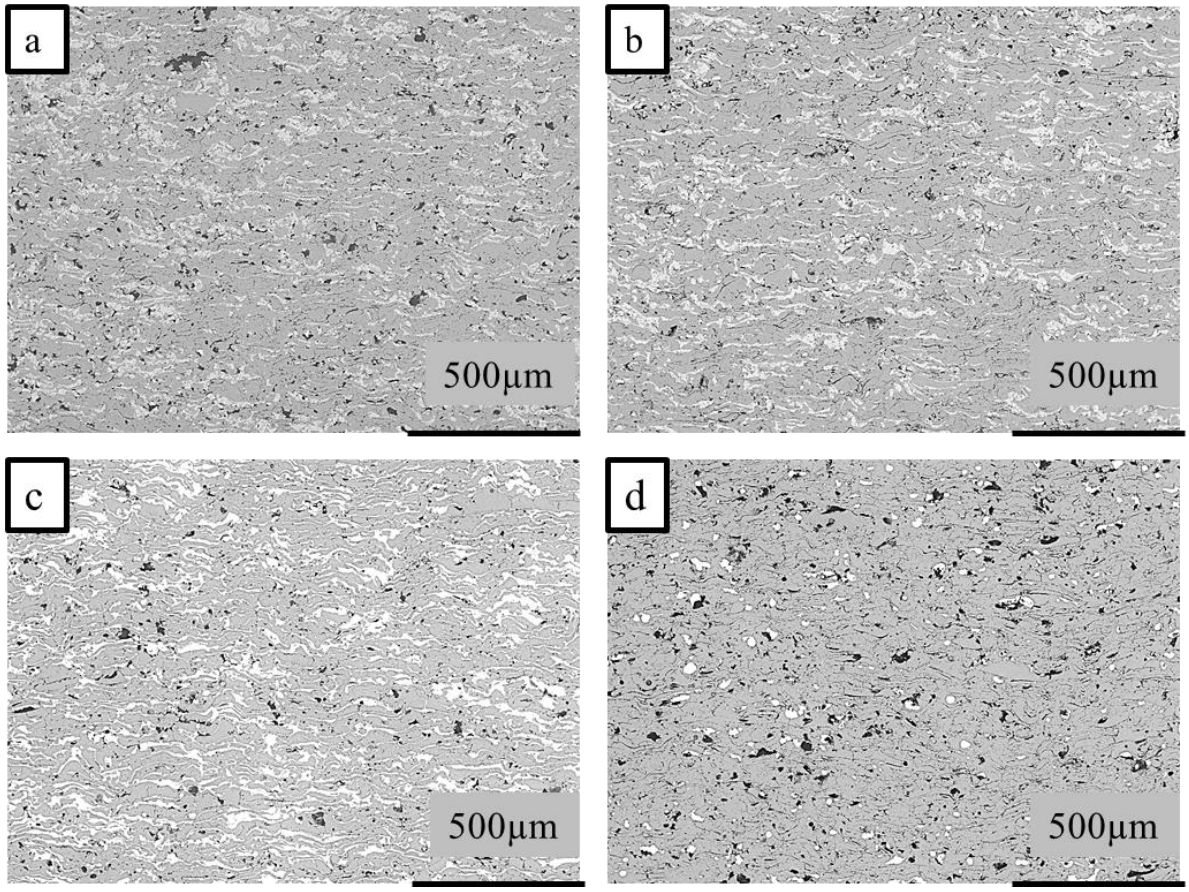

Figure 10.1: Microstructures of alumina hybrid composite with (a) aluminum, (b) aluminum with 5% Mg_2Si, (c) copper, and (d) nickel.

Initial testing of hybrid composites was done by using 3-point bending to test for both flexural strength and fracture toughness as well as the standard template without metal as shown in Figure 10.2. Copper reported the highest values in both in strength and toughness, while the aluminum and aluminum with 5% Mg_2Si were similar, which was expected. The Mg_2Si was added to enhance the effects during heat treatment which would be shown in later work. Surprisingly though, the as sprayed template and nickel hybrid composite gave quite similar results. This occurs due to the lack of metal and higher amounts of porosity in the alumina-nickel structure.

Instead of co-spraying with metals, there is the option of spraying another ceramic material to behave similar to that of a whisker and fiber composite. By applying another ceramic, the crack will have to propagate through alternating materials adding a toughening mechanism to the hybrid composite through either bridging or sliding. Similar to the metal composite, it is

important that the bonding between the layers is not too great such that interlayer sliding can occur.

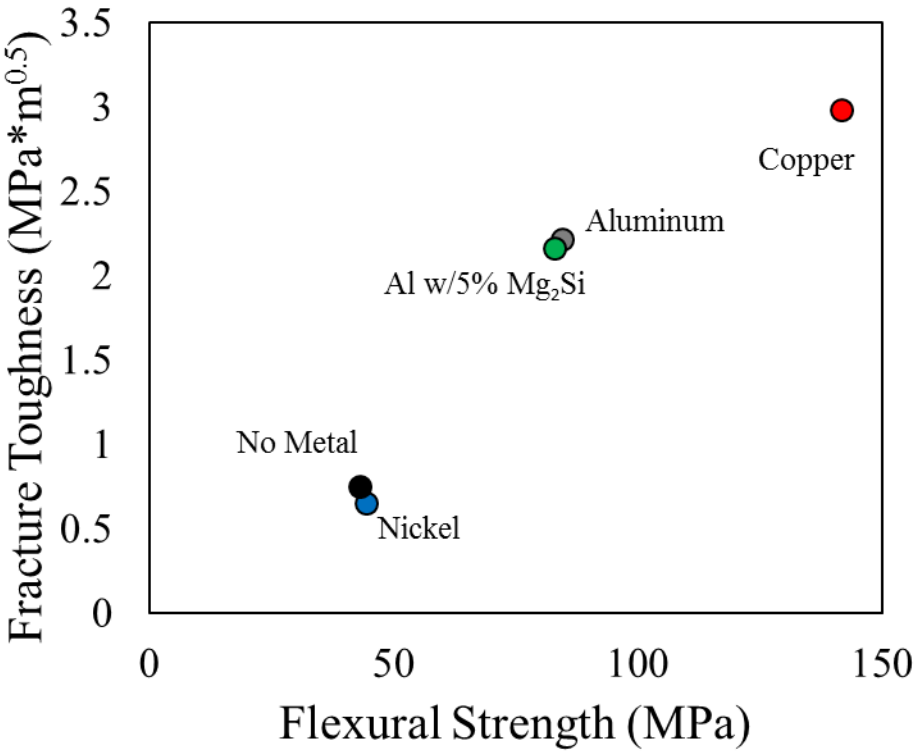

Figure 10.2: Fracture toughness vs. flexural strength plot of alumina hybrid composite with various metals and as well as the standard template without metal.

11 References

1. Anderson, T.L., *Fracture mechanics : fundamentals and applications*. 2005: CRC Press.
2. William D. Callister, J., *Materials Science and Engineering An Introduction*. 7 ed. 2007: John Wiley & Sons, Inc.
3. Irwin, G.R., *Onset of Fast Crack Propagation in High Strength Steel and Aluminum Alloys*. 1956, Naval Research Laboratory.
4. Launey, M.E. and R.O. Ritchie, *On the Fracture Toughness of Advanced Materials.* Advanced Materials, 2009. **21**(20): p. 2103-2110.
5. ASTM, *Standard Test Method for Linear-Elastic Plane-strain Fracture Toughness K1c of Metallic Materials*, in *E399*. 2012.
6. Ritchie, R.O., *Mechanisms of Fatigue Crack-Propagation in Metals, Ceramics and Composites - Role of Crack Tip Shielding.* Materials Science and Engineering a-Structural Materials Properties Microstructure and Processing, 1988. **103**(1): p. 15-28.
7. Evans, A., *The New High-Toughness Ceramics.* Metals Test Methods and Analytical Procedures Collection, 1989.
8. Ritchie, R.O., *The conflicts between strength and toughness.* Nature Materials, 2011. **10**(11): p. 817-822.
9. Marshall, D.B. and J.E. Ritter, *Reliability of Advanced Structural Ceramics and Ceramic Matrix Composites - a Review.* American Ceramic Society Bulletin, 1987. **66**(2): p. 309-317.
10. Mah, T., et al., *Room-Temperature Mechanical-Behavior of Fiber-Reinforced Ceramic-Matrix Composites.* Journal of the American Ceramic Society, 1985. **68**(1): p. C27-C30.
11. Mah, T., et al., *High-Temperature Mechanical-Behavior of Fiber-Reinforced Glass-Ceramic-Matrix Composites.* Journal of the American Ceramic Society, 1985. **68**(9): p. C248-C251.
12. Barthelat, F., *Nacre from mollusk shells: a model for high-performance structural materials.* Bioinspiration & Biomimetics, 2010. **5**(3).
13. Dwivedi, G., et al., *Bioinspired Hybrid Materials from Spray-Formed Ceramic Templates.* Advanced Materials, 2015. **27**(19): p. 3073-3078.
14. Munch, E., et al., *Tough, Bio-Inspired Hybrid Materials.* Science, 2008. **322**(5907): p. 1516-1520.
15. Barthelat, F., *Biomimetics for next generation materials.* Philosophical Transactions of the Royal Society a-Mathematical Physical and Engineering Sciences, 2007. **365**(1861): p. 2907-2919.
16. Espinosa, H.D., et al., *Merger of structure and material in nacre and bone - Perspectives on de novo biomimetic materials.* Progress in Materials Science, 2009. **54**(8): p. 1059-1100.
17. Barthelat, F. and H.D. Espinosa, *An experimental investigation of deformation and fracture of nacre-mother of pearl.* Experimental Mechanics, 2007. **47**(3): p. 311-324.
18. J.D. Currey, J.D.T., *The mechanical behavior of some Molluscan hard tissues.* Journal of Zoology, 1974. **173**(3): p. 395-406.
19. Smith, R.K.a.R.W., *Thermal Spray Forming of Materials.* Powder Metal Technologies and Applications, 1998. **7**: p. 408-419.
20. Herbert Herman, S.S., Robert McCune, *Thermal Spray: Current Status and Future Trends.* MRS Bulletin, 2000. **25**(7): p. 17-25.
21. R.C. Tucker, J., *Thermal Spray Coatings.* Surface Engineering 1994. **5**: p. 497-509.

22. Thorpe, M.L., *Thermal Spray: Industry in Transition.* Advanced Material Process, 1993. **143**(5): p. 50-56.
23. Davis, J.R., *Handbook of thermal spray technology*. 2004: ASM International.
24. Flynn, K., *Investigation of Bio-Inspired Hybrid Materials through Polymer Infiltration of Thermal Spray Formed Ceramic Templates*, in *Materials Science and Enginerring*. 2014, Stony Brook University.
25. Currey, J.D., *Mechanical-Properties of Mother of Pearl in Tension.* Proceedings of the Royal Society Series B-Biological Sciences, 1977. **196**(1125): p. 443-+.
26. Dwivedi, G., *On the Anelastic Behavior of Plasma Sprayed Ceramic Coatings: Observations, Characterizations, and Applications*, in *Materials Science and Engineering*. 2011, Stony Brook University.
27. M. Kachanov, I.T., B. Shafiro, *Effective Moduli of Solids With Cavities of Various Shapes.* Applied Mechanics Reviews, 1994. **47**(1S): p. S151-S174.
28. Kroupa, F. and J. Plesek, *Nonlinear elastic behavior in compression of thermally sprayed materials.* Materials Science and Engineering a-Structural Materials Properties Microstructure and Processing, 2002. **328**(1-2): p. 1-7.
29. Nakamura, T. and Y.J. Liu, *Determination of nonlinear properties of thermal sprayed ceramic coatings via inverse analysis.* International Journal of Solids and Structures, 2007. **44**(6): p. 1990-2009.
30. Liu, Y.J., et al., *Anelastic Behavior of Plasma-Sprayed Zirconia Coatings.* Journal of the American Ceramic Society, 2008. **91**(12): p. 4036-4043.
31. Yagmur, L., S. Fank, and B. Aydemir, *Effect of microstructure on modulus loss at flexural mode and stress in sensor materials.* Sensors and Actuators a-Physical, 2007. **136**(1): p. 261-266.
32. Walsh, J.B., *The effect of cracks on the uniaxial elastic compression of rocks.* Journal of Geophysical Research, 1965. **70**(2).
33. Marcio R. Loos, L.A.F.C., Sergio H. Pezzin, *The Effect of Acetone Addition on the Properties of Epoxy.* Ciencia e Technologia, 2008. **18**(1): p. 76-80.
34. International, A., *Standard Test Method for Measurement of Fracture Toughness*, in *E 1820*. 2003.
35. Florian Bouvilee, E.M., Sylvain Meille, Bertramd Van de Moortele, Adam J. Stevenson, Sylvain Deville, *Strong, Tough and Stiff Bioinspired Ceramics from Brittle Constituents* Nature Materials, 2014.
36. Damani, R.J., D. Rubesa, and R. Danzer, *Fracture toughness, strength and thermal shock behaviour of bulk plasma sprayed alumina - effects of heat treatment.* Journal of the European Ceramic Society, 2000. **20**(10): p. 1439-1452.
37. Damani, R.J. and E.H. Lutz, *Microstructure, strength and fracture characteristics of a free-standing plasma-sprayed alumina.* Journal of the European Ceramic Society, 1997. **17**(11): p. 1351-1359.
38. Sen, D. and M.J. Buehler, *Structural hierarchies define toughness and defect-tolerance despite simple and mechanically inferior brittle building blocks.* Scientific Reports, 2011. **1**.